DEVELOPMENTAL BIOLOGY 167, 529–548 (1995)

undulated Phenotypes Suggest a Role of *Pax-1* for the Development of Vertebral and Extravertebral Structures

SUSANNE DIETRICH AND PETER GRUSS

Abteilung für Molekulare Zellbiologie, Max-Planck-Institut für biophysikalische Chemie, Am Fassberg, D-37077 Göttingen, Federal Republic of Germany

Accepted October 6, 1994

undulated extensive **mice carry a deletion of at least 28.2 kb, removing the terminal *Pax-1* exon including the poly(A) signal. This mutation leads to a drastically reduced amount of *Pax-1* transcript. The similarity in phenotype between *un*^{ex} and the point mutation *un* suggests both to be functionally equivalent. A third mutant, *Undulated short tail*, harbors a deletion of at least 48.3 kb, eliminating the *Pax-1* locus as well as 38 kb of flanking sequences. Phenotypically, this mutant differs from *un* and *un*^{ex}. The comparative phenotype analysis of all *undulated* alleles revealed morphological alterations in the vertebral column, the sternum, the scapula, the facial skeleton, and the thymus that correspond to *Pax-1* expression domains. The vertebral column phenotype is characterized by the reduction of vertebral components. These reductions can be traced back to the delayed cell accumulation in the embryonic sclerotome while the principal organization of this tissue is maintained. The morphological alterations outside the vertebral column are likewise confined to size reductions. Therefore, *Pax-1* may exert similar functions in all of its expression domains.**

INTRODUCTION

Using a paired box probe of the *Drosophila gooseberry* gene in homology screens, the murine *Pax-1* gene was the first vertebrate paired box containing gene to be isolated in 1988 (Deutsch *et al.*, 1988). Meanwhile eight additional *Pax* genes have been found in the mouse genome, constituting the murine paired box containing gene family of transcription factors (for review see Gruss and Walther, 1992). Sequence comparison suggests the murine *Pax* genes to belong to four groups (Gruss and Walther, 1992): the first group encompasses *Pax-1* and possibly *Pax-9* (Wallin *et al.*, 1993), harboring a paired box and an octapeptide. *Pax-3* and *-7* encode a second type of paired domain and octapeptide, and in addition a paired type homeodomain. *Pax-2*, *-5* and *-8* harbor a paired box, octapeptide and a truncated homeobox, while the *Pax-4* and *Pax-6* genes carry a divergent paired and homeobox only. The same groups of paralogous *Pax* genes have been identified in humans, birds, zebrafish (reviewed in Gruss and Walther, 1992), and in *Xenopus* (Featherstone and Turner, 1991), suggesting that the *Pax* gene functions are conserved among vertebrates.

Within the family of *Pax* genes, *Pax-1* displays unique features not only by structural means. Like other *Pax* genes expressed along the anteroposterior axis of the embryo, no *Pax-1* expression could be detected in the central nervous system. More similar to the closest *Drosophila* relative *pox meso*, *Pax-1* is mainly active in mesodermal tissues, particularly the developing vertebral column (Deutsch *et al.*, 1988). Therefore the *Pax-1* gene has been thought to be a sclerotomal marker, involved in the development of cartilaginous structures (Balling *et al.*, 1988). Nevertheless, the gene is also expressed in the pharyngeal pouch endoderm and in facial structures (Deutsch *et al.*, 1988; Dietrich *et al.*, 1993; this study), arguing for a function in processes that take place in nonmesodermal tissues as well.

The spatial and temporal expression pattern of a gene may serve as one criterion to propose possible gene functions. More direct evidence can be obtained from phenotypes associated with functional mutations of the gene. In the case of *Pax-1* this mutation experiment was done by nature: the mouse mutant *undulated* carries a spontaneous point mutation in the paired box of *Pax-1* causing a single glycine–serine exchange (Balling *et al.*, 1988). As a consequence, the DNA binding specificity of the mutant protein *in vitro* is altered and the DNA binding affinity drastically reduced (Chalepakis *et al.*, 1991). Corresponding to the *Pax-1* expression in the developing vertebral column, homozygous *un/un* animals exhibit a characteristic shortened and kinky tail phenotype due to irregularly shaped vertebrae and intervertebral discs (Wright, 1947; Grüneberg, 1963). The skeletal malformations are most obvious in the lumbar region where the vertebral bodies are strongly reduced or absent

0012-1606/95 $6.00

(Wright, 1947; Grüneberg, 1963). The first alterations in the *un/un* axial skeleton have been depicted at the mesenchymal stage of vertebral column formation at Day 11.5 pc when the medial sclerotome fails to develop the cell dense anlage of the intervertebral disc (Grüneberg, 1954). Consequently, the *Pax-1* gene has been suggested to be required for the development of vertebral components by controlling the process of medial sclerotome differentiation (Balling *et al.*, 1988, 1992). However, predominant *Pax-1* expression in the intervertebral disc anlagen at Day 11.5 pc (Deutsch *et al.*, 1988; this study), and the absence of these structures in the mutants does not explain the loss of the vertebral body; it rather indicates that the role of the *Pax-1* gene during vertebral column formation is still unclear.

Besides the vertebral column, *undulated* mutant mice have been reported to present anatomical alterations of the shoulder girdle, where the acromion of the scapula is reduced or absent (Grüneberg, 1963). Furthermore, in these animals fusions of sternebrae have been found (Grüneberg, 1963), indicating the *undulated* phenotype to be pleiotropic. However, the connection between mutant phenotype and extravertebral regions of *Pax-1* action has not been determined, leaving open the question whether *Pax-1* plays a more general role during development.

Since 1947, three more mouse mutants have been described to be allelic with *un*, *undulated* minimal (un^m; Wallace, 1979, 1980) that is extinct, *undulated extensive* (un^{ex}; Wallace, 1979, 1980), and *Undulated short tail* (Un^s; Blandova and Egorov, 1975). Un^s is a semidominant mutation, already in heterozygotes leading to a more drastically reduced tail length compared to *un/un* (Blandova and Egorov, 1975; Balling *et al.*, 1992). In contrast to the latter, the trunk vertebral column is less severely affected. In homozygous condition the Un^s mutation is lethal (Blandova and Egorov, 1975; Balling *et al.*, 1992). Since in these animals the *Pax-1* paired box has been shown to be deleted, Un^s has been suggested to be a null allele (Balling *et al.*, 1992; Wallin *et al.*, 1993). However, due to the unknown size of the deletion the contribution of additional genes to the Un^s specific aspects of the phenotype cannot be excluded. In contrast to Un^s, un^{ex} animals display a mutant phenotype more similar to *un* (Wallace, 1979). Being slightly more pronounced than in *un/un*, the phenotype still has been described to be recessive, in newborn animals confining sagittally split vertebrae to the un^{ex}/un^{ex} homozygotes. However, the un^{ex} mutation itself is not known (Balling *et al.*, 1992). Therefore, the molecular characterization of this mutation should provide us with a basis to comparatively analyze the genotype-phenotype relationship in *undulated* mutant mice.

In this study we provide evidence that in un^{ex} the *Pax-1* gene is mutated, leading to a drastically reduced amount of *Pax-1* transcript. In all *undulated* alleles we investigated the vertebral column phenotypes as they are delineated from impaired sclerotome condensation, suggesting this step of axial skeleton formation to be an intrinsic, *Pax-1*-dependent program of the sclerotome. Mutant phenotypes of the sternum, the scapula, the facial skeleton, and the thymus could be attributed to *Pax-1* expression domains, demonstrating that the *Pax-1* gene exerts essential functions also outside the vertebral column.

ANIMALS, MATERIALS, AND METHODS

Animals

Wildtype control animals were obtained by breeding NMRI females with B6D2 males or mating C57bl/6 animals *inter se*, all of these lines derived from the Zentralinstitut für Versuchstierzucht (Hannover, FRG). *Undulated short tail* and *undulated extensive* mice were kindly provided by A. M. Malashenko, Krosnogorsk, Russia, and J. L. Cruickshank, Leeds, England, respectively. *Undulated* mice were purchased from the Jackson laboratory, Bar Harbor, Maine. From all *undulated* alleles colonies were established, leveling the background by outcrossing to C57bl/6 mice for one to three generations. *undulated extensive* mice were in addition outcrossed to NMRI, revealing no differences in phenotype compared to the C57bl/6 lines.

All mice were mated overnight, taking 12 AM of the morning of the vaginal plug as Day 0.5 pc. The age of the mutant litters was determined according to Kaufman (1992). The genotype of the mutant animals was defined by the breeding strategy, or, in case of heterozygote matings, by Southern analysis of the decidua or the spleen, assaying for the point mutation in the *Pax-1* gene of *un* and for the *Pax-1* deletions in un^{ex} and Un^s.

Materials and Methods

RNA preparation. Total cellular RNA from embryonic tails at Day 14.5 pc was isolated according to (Chomczynski and Sacchi, 1987). To separate the poly(A)$^+$ and poly(A)$^-$ fractions, the Oligotex-dT mRNA kit (Diagen) was used.

Northern analysis. Northern analysis was performed following (Ausubel *et al.*, 1987), using 30 μg of total cellular RNA and 5 μg of poly(A)$^+$ RNA per lane. The RNA was transferred onto Quiabrane membranes (Diagen) in 20× SSC following the manufacturer's instructions, hybridized in 0.5 *M* sodium phosphate (NaPi), 7% SDS, 1 m*M* EDTA at 65°C, and washed in 40 m*M* NaPi, 1% SDS at 65°C according to Church and Gilbert (1984). The radioactive probe was labeled by random oligo labeling

(Feinberg and Vogelstein, 1983) using the random prime kit (Amersham). The signal intensity was measured on a PH-5 densitometer (Vernon), referring to β-actin as internal control.

RNaseH blot. Thirty micrograms of total cellular RNA and 500 p*M* of the oligonucleotide SD15 (5′-GCCAATCTTATTTCGCAGGATGCGACTGATG-3′) were annealed and RNaseH was digested according to Carrazana *et al.* (1988). After phenol–chloroform extraction a Northern analysis was performed as described above.

RNase protection assay. Thirty micrograms of total cellular RNA and the corresponding poly(A)$^+$ and poly(A)$^-$ preparations, 1.5 and 28.5 μg, respectively, were supplemented with *Escherichia coli* tRNA to 40 μg and assayed according to Stamminger *et al.* (1990).

Whole mount in situ hybridization. The whole mount *in situ* hybridization procedure was performed according to Wilkinson (1992) using the Boehringer-Mannheim Digoxigenin system. The Proteinase K treatment lasted 10–15 min. After hybridization with the riboprobe and the anti-DIG antibody, respectively, the embryos were washed overnight. The staining of the animals was stopped with phosphate-buffered saline/Tween (PBT) after the signals appeared in the un^{ex}/un^{ex} animals. To control the specificity of the signals Un^s/Un^s embryos were analyzed in parallel.

Isolation of genomic DNA and Southern blot. Genomic DNA from the embryonic decidua or from the spleen of newborn mice was isolated according to Ausubel *et al.* (1987), subsequently digesting 5 μg with appropriate restriction endonucleases. After electrophoresis, the fragments were transferred to Qiabrane nylon membranes (Diagen) and hybridized with radiolabeled probes as described for the Northern analysis.

Sequence analysis. Double-stranded DNA cloned into pBluescript (Stratagene) was sequenced according to the dideoxy-nucleotide method, utilizing the T7-deaza sequencing kit from Pharmacia.

Pax-1 probes. The 35 kb upstream of the first *Pax-1* exon localized genomic g*Kpn*I probe encompasses 1.3 kb. The 556-nt g*Cla*I–*Bam*HI probe contains 279 nt of the 1st intron and 277 nt of the adjacent 2nd exon, including parts of the paired box. The 313-nt c*Hinc*II–*Sac*I probe is entirely exon 2-derived as described in Deutsch *et al.* (1988). The 488-nt c*Sma*I-2 probe corresponds to position 824–3113 of the cDNA, thus harboring sequences from the 2nd to 4th and 26 nt of the last exon. The 326-nt g*Sty*I–*Dde*I probe encompasses parts of the 3rd and 4th introns, as well as the intervening 217 nt of exon 4. The 1.7-kb g*Eco*RI probe is localized in the middle of exon 4, 2 kb 3′ of the 4th exon, containing the 302-nt g*Eco*RI–*Bsp*HI subfragment at its 5′ end. The 1.19-kb g*Bam*HI–*Nhe*I probe corresponds to the 3′ portion of exon 4 and to 180 nt at the 5′ end of exon 5. The 349-nt c*Ssp*–*Alu*I probe is derived from the *Pax-1* cDNA positions 2094–2443. The genomic g*Kpn*I–*Bam*HI probe encompasses 1.3 kb, localized 4.9 kb downstream of the *Pax-1* exon No.5.

Pax-8 probe. A 914-nt PCR product corresponding to the cDNA positions 130–1043 as described in Plachov *et al.* (1990) was used.

Skeletal preparations. Skeletal preparations were performed according to Kessel *et al.* (1990). To photograph the skeletons ventrally, internal organs were removed. In newborn mice, in addition, the ventral parts of the ribcage were removed and the extremities disarticulated.

Sections and hematoxylin/eosin staining. The embryos were embedded in Paraplast plus according to Kaufman (1992) and the lumbar region coronally sectioned to 5 μm on a Reichert–Jung 2040 microtome. Similarly, frontal sections were taken from the thymus of newborn animals. The sections were collected on gelatinized slides, HE-stained according to (Romeis, 1989), and covered with Eukitt (Kindler).

Microscopy and photography. Skeletons were photographed on a Zeiss Stemi SV8 binocular microscope and whole mounted embryos and HE-stained sections on a Zeiss Axiophot microscope using bright-field or Nomarski optics.

RESULTS

Molecular Analysis of the undulated extensive Mutation

To determine whether the *Pax-1* gene is mutated in un^{ex}/un^{ex} mice, the structure of the gene was investigated by Southern analyses. Probes derived from upstream regions (not shown) as well as exons 1–4 lead to the same restriction pattern both in wildtype and un^{ex}/un^{ex} animals (Fig. 1A). The intron 4-derived probe depicts restriction fragment-length polymorphisms after digestion with *Xba*I, *Eco*RI, and *Xho*I plus *Kpn*I (Fig. 1B). Fine mapping revealed that in the middle of the 4th intron, within a 365-nt region at the 3′ end of the *Eco*RI fragment, any homology between wildtype and mutant sequences is lost (not shown). Probes derived from the 3′ end of this intron, from the last exon and 4.9 kb 3′ of the terminal exon do not hybridize to the un^{ex}/un^{ex} genome, indicating a deletion of at least 15.7 kb (Figs. 1C and 1D). In these animals, in 9.1 kb proximity to the 4th *Pax-1* exon and about 6.3 kb apart from the 5′ breakpoint of the deletion a *Sma*I site is located that is not represented in the 24.9 kb of available 3′ cosmid sequences (not shown). Similarly, 12.6 kb 3′ of exon 4 and 9.8 kb 3′ of the breakpoint of the deletion a *Cla*I site are found, while the wildtype-specific *Xho*I site about 20.2 kb 3′ of the 5th exon is absent (Fig. 2). Consequently, the deletion in the *Pax-1* region of un^{ex}/un^{ex} measures at least 28.2 kb, removing the last exon of the gene and the polyadenylation signal.

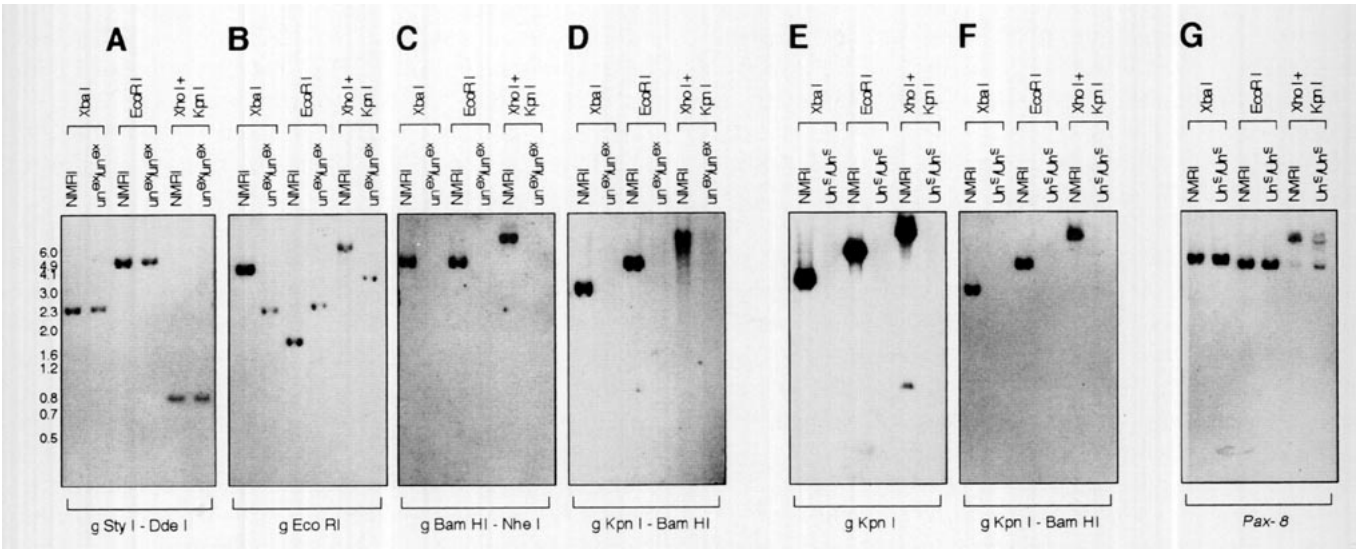

FIG. 1. Southern analysis of the *Pax-1* gene structure in un^{ex}/un^{ex} and Un^s/Un^s. (A) Hybridization with the a probe spanning exon 4 and parts of the flanking intron sequences results in the same pattern of restriction fragments in NMRI and un^{ex}/un^{ex}. (B) The 2 kb 3′ of the 4th exon-located intron 4 probe hybridizes to different restriction fragments in +/+ and un^{ex}/un^{ex}. Hybridization with the intron 4–exon 5-derived probe (C) and a genomic probe located 4.9 kb 3′ of the 5th exon (D) indicates a deletion of these sequences in un^{ex}/un^{ex}. Hybridization of +/+ and Un^s/Un^s DNA preparations with probes derived from the 5′ (E) and 3′ (F) flanking regions of the *Pax-1* locus. In Un^s/Un^s, the entire *Pax-1* gene including these flanking sequences is deleted. (G) Control hybridization of the blot in (E,F) with a *Pax-8* probe, like *Pax-1* located on mouse chromosome 2.

RNase protection analyses of Day 14.5 pc tail RNAs showed that the deletion within the un^{ex}/un^{ex} genome leads to an altered structure of *Pax-1* mRNAs: the molecules lack sequences derived from the 3′ terminal exon. As expected, the exon 2–5 encompassing cDNA probe becomes shortened by the exon 5 encoded portion (Fig. 3B), and the probe derived solely from this exon is not protected at all (Fig. 3D). Instead, positive signals can be obtained using an intron 4-derived probe, which is located about 2 kb 3′ of the 4th exon and about 1.2 kb 5′ of the deletion (Fig. 3C). Similarly, sequences derived from the 5′ end of this intron are represented (not shown), suggesting that in contrast to +/+ and *un/un* at least a majority of $un^{ex}/Pax\text{-}1$ transcripts remains improperly spliced.

At the 5′ end, the $un^{ex}/Pax\text{-}1$ transcripts resemble wildtype molecules. Using a genomic probe derived from the intron–exon boundary of the 2nd exon, the same protected fragment can be observed in un^{ex}/un^{ex} and the wildtype controls (Fig. 3A). Similarly, if, prior to Northern analysis, the RNA preparations are hybridized with an oligonucleotide complementary to the 3′ region of the paired box (SD15), followed by removal of the 3′ portions of the *Pax-1* mRNA by cutting the double-stranded region with RNaseH, the 666-nt fragment corresponding to the 5′ end of the *Pax-1* transcript can be found in un^{ex}/un^{ex}, *un/un*, and +/+ (Fig. 4A). However, in both types of assays the intensity of the un^{ex}/un^{ex} signal is drastically reduced. Densitometric evaluation of the RNaseH blots referring to the β-actin signal as an internal con-

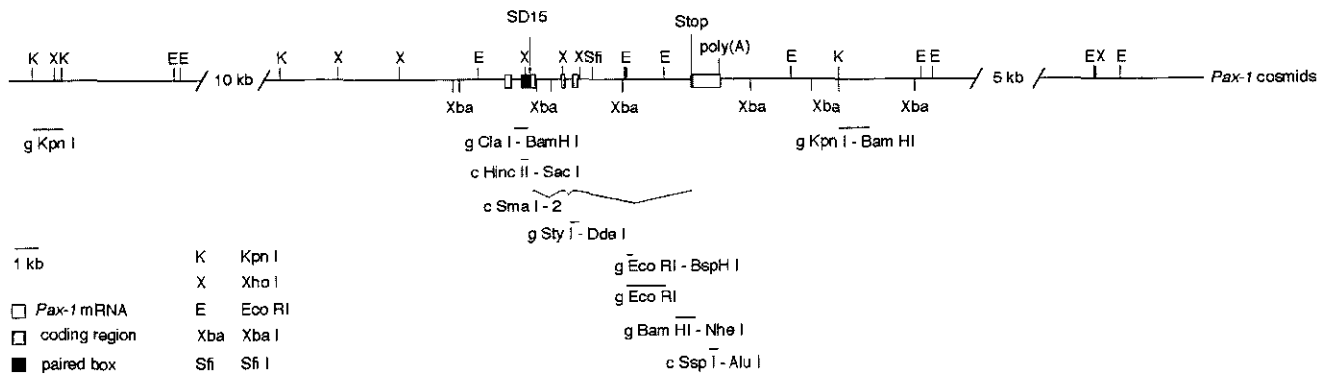

FIG. 2. Map of the *Pax-1* locus on chromosome 2 adapted from Deutsch (1990) and the probes used in this study.

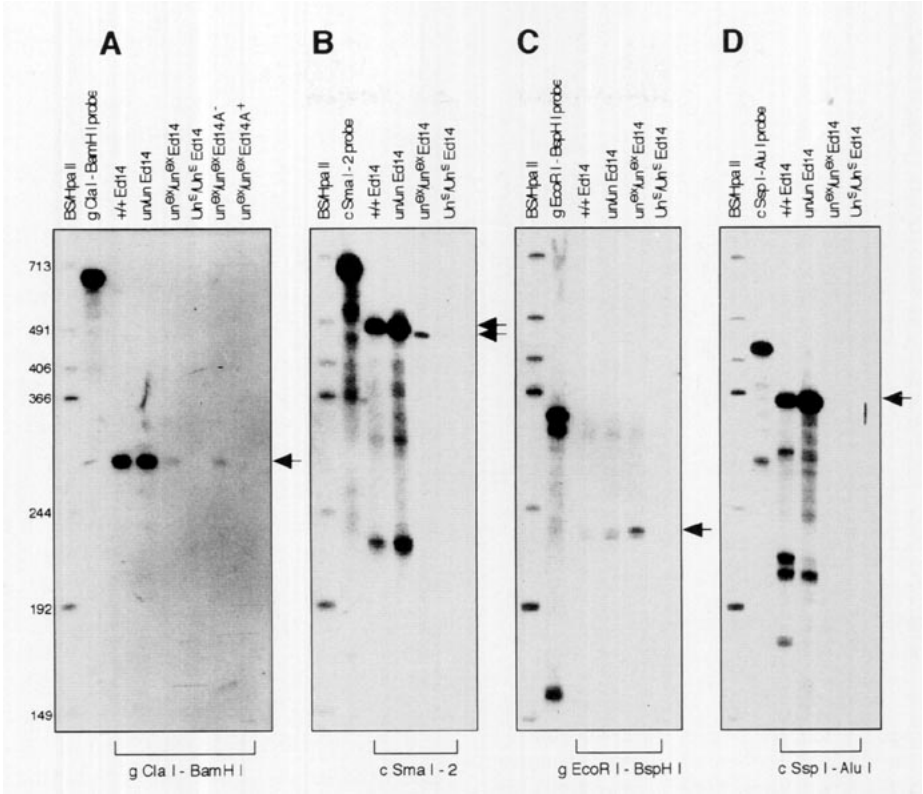

FIG. 3. RNase protection analysis of the *Pax-1* mRNA structure in wildtype and *undulated* tails at Day 14.5 pc. The positions of the probes are indicated in Fig. 2. (A) Hybridization with an intron 1–exon 2-derived probe. Note the signal obtained with total cellular and poly(A)$^-$ RNA preparations from un^{ex}/un^{ex} embryonic tails. Compared to +/+, the intensity of this signal is reduced. (B) Hybridization with an exon 2–5 spanning cDNA probe. The protected fragment in un^{ex}/un^{ex} is shorter than that in +/+. The size difference corresponds to the length of the exon 5-derived portion of the probe. (C) Hybridization with a 2-kb downstream of the 4th exon-located intron 4 probe. Note the strong signal in the un^{ex}/un^{ex} lane. (D) The exon 5-derived cDNA probe does not hybridize to the un^{ex}/un^{ex} RNA preparation.

trol indicated that the intensity of the *Pax-1* signal reaches about 25% of the wildtype level in un^{ex}/un^{ex} and about 70% in $un^{ex}/+$.

Without RNaseH treatment, no transcription of the $un^{ex}/Pax\text{-}1$ gene is detectable by Northern analyses, neither with total cellular nor using poly(A)$^+$ RNA (Fig. 4A). This finding suggests that the 3′ portion of the transcripts and consequently their overall size is heterogeneous, during electrophoresis resulting in the distribution of the molecules throughout the lane. However, positive signals can be obtained in RNase protection assays using poly(A)$^-$ preparations of un^{ex}/un^{ex} RNA only (Fig. 3A). Thus, the deletion of the exon 5 encoded poly(A) signal leads to poly(A)-deprived mRNAs, suggesting that accelerated RNA degradation accounts for both length variation and low abundance of the molecules.

As the 5th *Pax-1* exon encodes the 30 C-terminal amino acids, un^{ex}/un^{ex} mice were expected to express an altered *Pax-1* protein. Sequence analysis of the intron 4 portion represented in the mutant RNA shows that 3′ of exon 4 the open reading frame is extended by 30 amino acids (Fig. 5). Therefore, the mutant protein should exhibit wildtype length but a different amino acid composition. Nevertheless, using the polyclonal anti *Pax-1* serum no protein could be detected at all, neither in Western nor in whole mount analysis of un^{ex}/un^{ex} embryos (not shown). However, since 9 of 14 amino acids used as a polypeptide antigen are encoded by the deleted exon 5 (Chalepakis *et al.*, 1991), this antiserum might fail to recognize the mutant *Pax-1* protein. Alternatively, low abundance and structural changes of the transcripts may prevent the effective production of *Pax-1* proteins in un^{ex}/un^{ex} mice.

Molecular Analysis of the Undulated short tail Mutation

Un^s/Un^s mice have been suggested to represent a *Pax-1* null allele, due to the deletion of the paired box (Balling *et al.*, 1992; Wallin *et al.*, 1993). To compare the mutations in un^{ex}/un^{ex} and Un^s/Un^s, we extended the molecular characterization of the latter. RNA preparations of Un^s/Un^s embryos are completely deprived of *Pax-1* sequences (Figs. 3 and 4), confirming the classification as a null allele. Moreover, Southern analyses showed that all probes derived from the *Pax-1* locus fail to hybridize to the Un^s/Un^s genome (Figs. 1E–1G). Consequently,

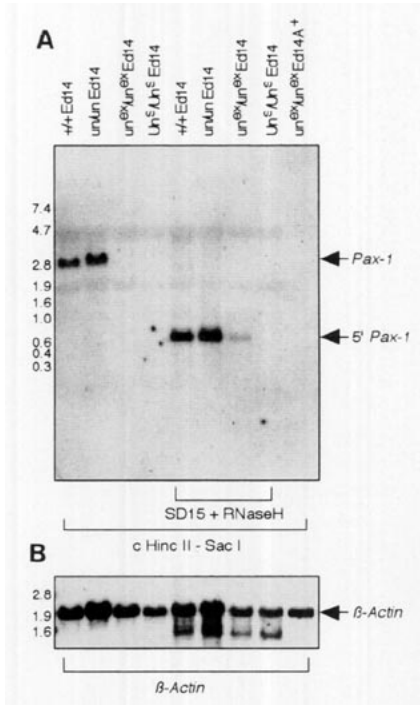

FIG. 4. Northern and RNaseH analysis of *Pax-1* transcripts in wild-type and *undulated* tails at Day 14.5 pc. Using a paired box derived probe, a weak *Pax-1* signal appears in the un^{ex}/un^{ex} lane after removal of the 3′ portion of the mRNA. The signal intensity compared to +/+ is drastically reduced. Without RNaseH treatment, this signal is not detectable at all.

these mice carry a deletion of at least 48.3 kb removing the entire *Pax-1* gene and about 38 kb of flanking sequences. As the breakpoints of the deletion could not be identified yet, additional genes may be affected as well.

Comparative Vertebral Column Analysis of undulated Mutant Mice

The analysis of the *Pax-1* gene in *undulated extensive* illustrated that in all *undulated* alleles the *Pax-1* gene is mutated. To study the genotype-phenotype relation, we comparatively analyzed anatomical alterations in all alleles in heterozygous and homozygous condition, as well as in the compound heterozygotes in all permutations. Since the phenotype of the compound heterozygotes remained invariant, independent from the transmission of the stronger allele through the maternal or paternal germline thus excluding imprinting, in the following we will only refer to the three possible compound genotypes as such.

The vertebral column phenotypes were investigated in alcian blue/alizarin red-stained skeletons of newborn and 13.5-day-old animals, scoring presence, reduction, or absence of vertebral column components between the 1st cervical (C1) and the 10th caudal vertebra (Ca10). Embryos at Day 12.5 pc were similarly analyzed between C1 and Ca2. Atlas–axis fusion were not taken into account, since in the background line C57bl/6 8% of the animals also developed this phenotype.

un/+ and un^{ex}/+ heterozygotes displayed the weakest phenotypes (Table 1). Sixteen percent of the newborns showed single lumbar vertebrae with anteroposteriorly and dorsoventrally reduced vertebral bodies, irregular intervertebral discs, shortened transverse processes, and weakened neural arches (not shown). At Day 13.5 pc reduced or sagittally split lumbar vertebral bodies were found in 45% of these animals, while at Day 12.5 pc 85% exhibited this phenotype (not shown), encompassing a wider region than at Day 13.5 pc. In the center of this zone, split vertebrae may lack the ventromedial components completely, consequently not reaching the notochord. However, as this phenotype is compensated during development, the formation of ventromedial vertebral column appears delayed rather than blocked.

In *un/un* and un^{ex}/un^{ex} homozygotes, and un/un^{ex} compound heterozygotes, skeletal aberrations are found at any of the analyzed stages and at any axial position (Fig. 6B, Table 1). In newborns, mildly affected vertebrae are restricted to the upper thoracic region, where the vertebral bodies are reduced in anteroposterior and dorsoventral dimension, ossifying from reduced centers. In the lower thoracic, the lumbar, and the sacral regions, the vertebrae lack their centers but remain ventrally closed due to the fusion of the pedicles. Here, the intervertebral discs disappear as well. In the lumbar region, the pedicles may fail to fuse across the ventral midline, unable to compensate the loss of the vertebral body. These pedicles may ventrally be connected by irregularly shaped cartilage, that often fused to the neighboring cartilaginous structures. Their texture resembles the not yet ossified, most ventrolateral portion of the pedicles in wildtype mice rather than intervertebral discs, suggesting that the mutant lumbar vertebrae are entirely deprived of their ventromedial components. This interpretation is supported by the inspection of disarticulated lumbar vertebrae: they lack vertebral bodies and intervertebral discs (Figs. 6F and 6G).

In the lumbar region, in addition to the ventromedial components, the transverse processes are either reduced or absent; rudiments may alter their orientation due to neural arch narrowing (Figs. 6B, 6F, and 6G). Similarly affected ventrolateral axial skeleton components can be observed in the lowermost thoracic region, where the ribs may be stiffly connected or even unconnected with the corresponding vertebrae. In posterior body regions, neural arches occasionally fail to fuse dorsally (not shown), indicating that even dorsolateral components of the vertebral column may be compromised.

Compared to the newborn stage, *un/un*, un^{ex}/un^{ex} and

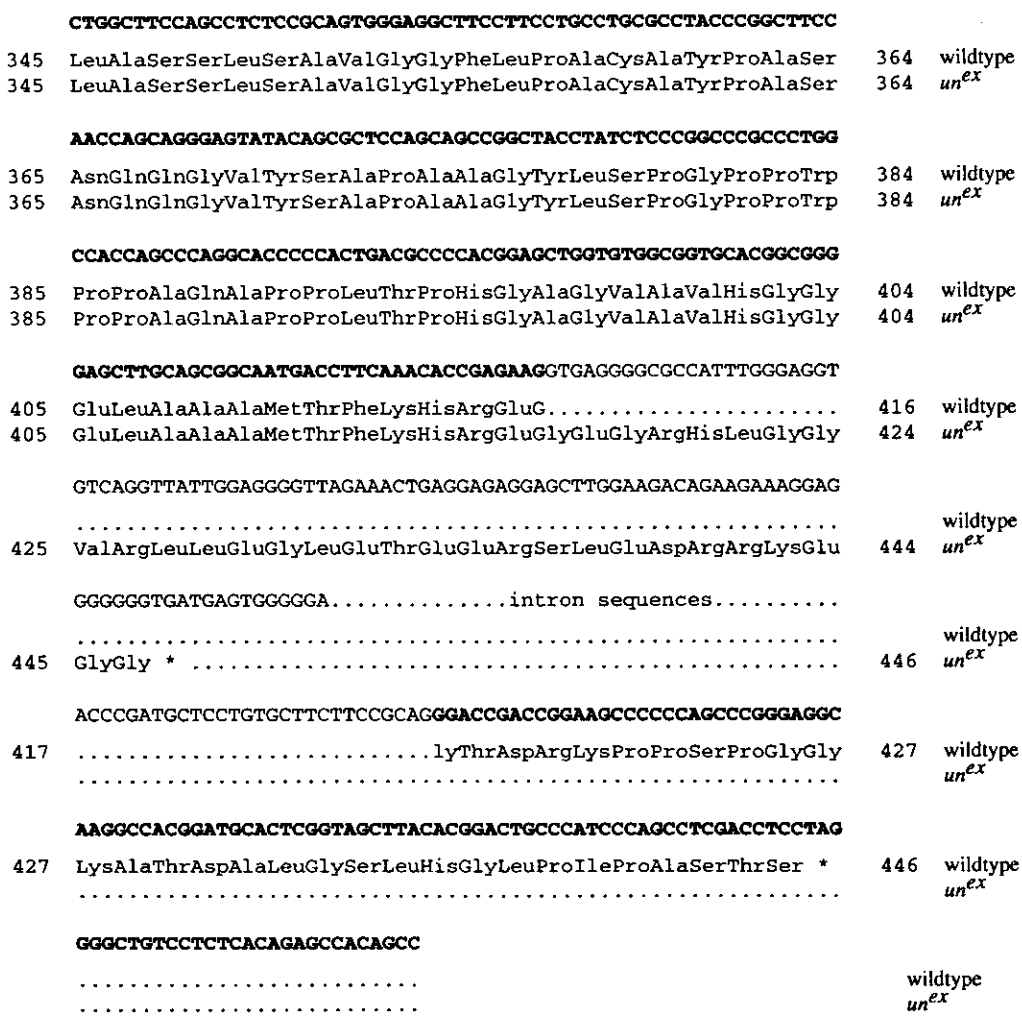

FIG. 5. Coding region of the 4th exon, the adjacent intron, and the 5th exon; stop codons are indicated by a star. Note that in the putative un^{ex}/*Pax-1* protein the C-terminus is replaced by intron 4 encoded sequences.

un/un^{ex} embryos again exhibit a stronger phenotype (Table 1). At Day 12.5 pc sagittally split vertebrae are found in the lower thoracic, the entire lumbar and the upper sacral vertebral column (not shown). In addition, in some embryos split cervical vertebrae have been observed, confirming the idea of partial mutant phenotype compensation during development. In the lumbar region, the strongest affected vertebrae completely lack the anlage of the vertebral body. Here, the pedicles do not reach the ventral midline even at Day 13.5 pc (Fig. 6K), illustrating that the formation of ventromedial vertebral components is more retarded than in the heterozygotes. On average, the left half of the neural arch more frequently fails to ventromedially reach the notochord than the right, possibly due to the flexure of the embryos predominantly to the right side applying more physical stress to the left.

While in the *un* and un^{ex} alleles the most dramatic phenotypes are found in the lumbar region, in $Un^{s}/+$ heterozygotes the tail is most strongly affected, appearing even more drastically shortened than in un^{ex}/un^{ex} due to vertebral reduction and multiple fusions (not shown). Within the trunk all vertebral bodies are similarly reduced in anteroposterior, dorsoventral, and mediolateral dimension (Table 1), and the intervertebral discs exhibit a lentil-shaped morphology (not shown). In addition, all neural arches are narrowed. The 13th rib exhibits a slender morphology, while the proximal portion of the 9th or 10th rib appears strongly ventrally bent. In the lumbar region the vertebrae are deprived from transverse processes; posteriorly, no sacrum is formed. As in contrast to the former alleles the ventrolateral phenotypes does not coincide with the absence of ventromedial structures, the $Un^{s}/+$ mutation may cause a more general underdevelopment of vertebrae. However, at embryonic stages $Un^{s}/+$ mutants exhibit sagitally split vertebrae similar to $un/+$ and $un^{ex}/+$, though the penetrance of this phenotype is complete

TABLE 1
TYPE AND FREQUENCY OF VERTEBRAL COLUMN PHENOTYPES IN *undulated* MUTANT MICE

Mutant	Stage	Number of animals	% animals with mutant phenotype	Number of vertebrae/animal with		
				Ventromedial reductions	Ventromedial clefts	Retrosomatic clefts
un/+	NB0	9	11	0.1	0	0
	E 13.5	29	31	1.7	0	0
	E 12.5	5	100	0.6	1.6	nd
un^{ex}/+	NB0	14	21	0.4	0	0
	E 13.5	26	58	1.1	0	0
	E 12.5	16	69	4.4	2.1	nd
un/*un*	NB0	3	100	37.7	2.3	0
	E 13.5	20	100	36.5	3.5	0
	E 12.5	4	100	19.8	12.2	nd
un^{ex}/un^{ex}	NB0	7	100	37.9	2.1	0
	E 13.5	6	100	35.8	4.2	0
	E 12.5	10	100	19.7	12.3	nd
un/un^{ex}	NB0	7	100	38.6	1.4	0
	E 13.5	12	100	36.9	3.1	0
	E 12.5	10	100	25.3	6.7	nd
Un^{s}/+	NB0	2	100	40.0	0	0
	E 13.5	15	100	5.8	0.1	0
	E 12.5	11	100	20.3	4.8	nd
Un^{s}/Un^{s}	NB0	2	100	24.0	16.0	12
	E 13.5	5	100	22.2	17.8	7.6
	E 12.5	3	100	7.0	25.0	nd
un/Un^{s}	NB0	5	100	29.4	10.6	4.8
	E 13.5	8	100	28.9	11.1	2.0
	E 12.5	7	100	14.3	17.7	nd
un^{ex}/Un^{s}	NB0	5	100	30.4	9.6	0.6
	E 13.5	8	100	29.1	10.9	1.63
	E 12.5	3	100	16	16	nd

Note. In newborn and Day 13.5 pc animals all 40 vertebrae between the 1st cervical and the 10th caudal vertebra were quantitatively analyzed for ventromedial vertebral reductions, visible as constrictions, ventral sagittal, and retrosomatic clefts. Similarly, in Day 12.5 pc embryos all 32 positions between C1 and Ca2 were investigated. At this stage, caudal retrosomatic cleft phenotypes could not be determined due to incomplete cartilage formation. Note that *un*/+ and un^{ex}/+ develop analogous phenotypes. The same applies to *un*/*un*, un^{ex}/un^{ex}, and un/un^{ex}, whilerQun/Un^{s} and un^{ex}/Un^{s} resemble Un^{s}/Un^{s}. In all mutants the most extreme phenotypes are confined to Day 12.5 pc.

(Table 1). Again, split vertebrae are most frequent at Day 12.5 pc.

In contrast to the mutants described so far, the un/Un^{s}, un^{ex}/Un^{s} and Un^{s}/Un^{s} genotypes lead to lethality briefly after birth. Rarely, compound heterozygotes survived to juvenile ages, remaining very small and suffering from strong kyphoses and scolioses. Skeletal preparations of newborn animals revealed absence of intervertebral discs and sagittally split vertebrae in the cervical region, the lower thoracic, the lumbar, and the upper sacral regions, leaving expanded sectors of the vertebral column ventrally open (Fig. 6C, Table 1). Occasionally, the lateral parts of these vertebrae are attached to ventromedial stripes of cartilage that represent a persisting notochord and possibly rudimentary ventromedial or ventrolateral sclerotomal tissues. In the most strongly affected region, in addition to absent vertebral bodies the pedicles are drastically shortened or absent and the lamina narrowed. The extinction of ventrolateral axial skeleton components includes the proximal parts of the lowest ribs, which are consequently not attached to the vertebral column. This phenotype, together with a curvature of the 8–9th rib more pronounced than in Un^{s}/+, leads to a flattened ribcage that may account for breathing problems and the neonatal death. In the lumbar region, the loss of ventrolateral structures encompasses the transverse processes. Posteriorly, the animals do not develop the sacrum, rem-

FIG. 6. Skeletal preparations of wildtype and *undulated* mutant mice at birth and Day 13.5 pc. The scale bar in (A) represents 3.5 mm in (A–C), the scale bar in (D) 400 μm in (D–I), and the scale bar in (J) 650 μm in (J–L). C, notochord; V, vertebral body, P, pedicle; La, lamina; 1, transverse process; 2, processus articularis superior; 3, processus articularis inferior; 4, anlage of the spinous process; I, intervertebral disc; R, rib; C1, 1st cervical vertebra; T1, 1st thoracic vertebra; L1, 1st lumbar vertebra; S1, 1st sacral vertebra; Ca1, 1st caudal vertebra; the positions of sagittally split vertebrae are indicated. (A–C) Newborn animals, ventral view; ribcage and limbs removed. (A) +/+. Note the separate ossification centers in the vertebral bodies and in the neural arches. (B) un^{ex}/un^{ex}. The vertebral bodies are drastically reduced or absent. In the thoracic and sacral region, the loss of the vertebral body is compensated by ventrally closed neural arches. Failure of the lumbar neural arches to reach the ventral midline leads to sagittally split vertebrae as indicated for L4 and L5. The with respect to the animal right, 13th rib is stiffly connected to the corresponding vertebra while the left counterpart shows no vertebral connection at all (R). (C) Un^{s}/Un^{s}. Sagittally split vertebrae are found in the cervical region and in the lower thoracic and the lumbar vertebral column from T10-L4/5. The vertebral rudiments are often fused to their neighbors (f). Note the median stripe of cartilage (m) probably representing the persisting notochord. In the caudal region only the pedicles are absent, causing retrosomatic clefts (arrows). The ribs appear broadened and strongly ventrally bent. The lowest ones fail to contact the vertebral column, and the 13th pair of ribs is missing (R). (D–I) preparations of the 5th lumbar vertebrae; (D, F, H) view from anterior, dorsal to the top; (E, G, I) lateral view, anterior is to the left. (D, E) +/+. (F, G) un^{ex}/un^{ex}. The vertebral body is absent (arrow), the pedicles hardly reach the ventral midline, and the lamina appear slightly dorsally shortened. The drastically reduced transverse processes point posterior due to the narrowed neural arches (small arrows). (H, I) Un^{s}/Un^{s}. Strongest phenotype: agenesis of vertebral body (arrow), pedicle, and transverse process (small arrow). The ventrally located cartilaginous structure (m) may result from notochord persistence. The articulation processes appear short and poorly differentiated. The lamina are shortened, leading to dorsal dyssymphysis (arrowhead). (J–L) Embryos Day 13.5 pc, ventral view. (J) +/+. In the trunk, vertebral bodies, pedicle, and the ventral portions of the laminae are preformed in cartilage. (K) un^{ex}/un^{ex}. Vertebral bodies are absent from the lower thoracic to the sacral region. Lumbosacrally, the pedicles do not reach the notochord. Note that the zone of sagittally split vertebrae is wider than in the newborn. (L) Un^{s}/Un^{s}. Sagittal vertebral clefts are found cervically and in a wide zone from T10-S2/3. Note the caudal retrosomatic clefts (arrow) and the frequent vertebral fusions (f). The lowest ribs lack the proximal portion, and the 13th pair is completely absent (R).

FIG. 7. Sclerotome of wild-type and *undulated* embryos at Days 10.5 and 11.5 pc. Hematoxylin/eosin-stained 5-μm coronal sections of the lumbar region; anterior is to the top. The scale bar in (A) represents 100 μm in (A–D). C, notochord; D, dermatome; M, myotome; Sc, sclerotome; Sp, spinal nerve; a, anterior sclerotome half; p, posterior half; l, lateral sector; m, medial sector: The arrows indicate the segmental (somitic) borders. (A, B) Embryos Day 10.5 pc. (A) +/+. Note the condensing mesenchyme in the posterior half of the lateral sclerotome (arrows). (B) un^{ex}/un^{ex}. The lateral sclerotome condensations appear retarded (arrowheads). (C, D) Embryos Day 11.5 pc. (C) +/+. Note the cell condensations in the medial aspect of the sclerotome: In the posterior sclerotome half, the cell dense zone is continuous with the lateral condensation (arrowhead). A second condensing zone is located intrasegmentally, directly adjacent to the posterior half (arrowhead). (D) *un/un*. A small stripe of condensing cells within the posterior sclerotome half is visible. It hardly reaches the notochord. The intrasegmental condensation has not formed yet. The arrowheads indicate the missing condensations.

FIG. 8. The sclerotomal *Pax-1* expression pattern in the lumbosacral region of embryos at Days 10.5 and 11.5 pc. Whole mount *in situ* analysis; the neural tube is removed. The scale bar in (A) represents 100 μm in (A–D); abbreviations as in Fig. 7. (A) +/+ Day 10.5 pc, dorsal view into the grove obtained from neural tube removal, anterior is to the top. Elevated levels of *Pax-1* expression are confined to the posterior half of the lateral sclerotome (arrowheads). (B) un^{ex}/un^{ex} Day 10.5 pc, same view as in (A). The region of strong *Pax-1* expression is narrowed (arrowheads). (C) +/+ Day 11.5 pc, same view as in (A). Intense *Pax-1* expression in the posterior and the intrasegmental portion of the sclerotome (arrowheads). Note that the extraordinarily strong lateral staining is partly due to the sclerotome thickness being maximal in this region. (D) *un/un* Day 11.5 pc, same view as in (C). Strong *Pax-1* expression is restricted to a narrow zone within the posterior sector of the sclerotome (arrowheads).

FIG. 9. Extravertebral *undulated* phenotypes. (A–C) Sternum and rib cage preparations of newborn wildtype, un^{ex}/un^{ex}, and Un^{s}/Un mice. Dorsal view, the ribs are cut and the clavicle disarticulated, and anterior is to the top. The scale bar in (A) represents 1330 μm in (A, B). Ma, manubrium sterni; Co, corpus sterni; St, sternebra; X, xiphoid process; R1–R7, sternal ribs. (A) +/+ The lowest rib and the xiphoid process form an angle of about 52°. At the sternum–rib junctions the sternum remained cartilaginous, indicating the subdivision into sternebrae. The arrowhead marks the previous articulation with the clavicle. (B) un^{ex}/un^{ex}. The angle between the seventh rib and the xiphoid process is extended to about 58°. The arrowhead indicates fused sternebrae. The hole in the xiphoid process probably results from incompletely fused sternal bands (arrow). (C) Un^{s}/Un^{s}. The five lowest ribs and the xiphoid process form an angle of about 90°. The xiphoid process itself is broadened and terminally split (arrow). Similarly, the sternal bands between the 4th and 6ths ribs appear incompletely united. Here, two sternebrae are fused (arrowhead). (D–F) *Pax-1* expression and mutant phenotype in the appendicular skeleton. (D) Whole mount *in situ* analysis of the *Pax-1* activity in the forelimb of a Day 12.0 pc +/+ embryo, dorsolateral view, anterior is to the top, proximal to the left. The scale bar in (D) represents 340 μm. F, forelimb. Note the signals in the scapular area at the anterior and posterior margin of the forelimb (arrowheads). (E, F) Scapula and clavicle preparations of wildtype and un^{ex}/un^{ex} newborns. View from anterior, the lateral portion is to the top. The scale bar in (E) represents 870 μm in (E, F). Cl, clavicle; Pc, processus coracoideus; Ac, acromion; Spi, spina scapulae; Sca, blade of the scapula; l, lateral; m, medial; v, ventral; d, dorsal. (E) +/+. (F) un^{ex}/un^{ex}. The acromion is lacking (arrowhead) and the spina scapulae reduced (arrow). (G–I) Facial *Pax-1* expression and mutant skull phenotype. (G, H) Whole mount *in situ* analysis of the wildtype *Pax-1* expression in the embryonic face, Day 12.0 pc. The scale bar in (G) represents 810 μm in (G, H). Mxp, maxillary process of the first branchial arch; Np, nasal process; Nl, nasolacrimal groove; Mnp, mandibular process of the first branchial arch. (G) Frontal view, (H) lateral view. Note the *Pax-1* expression in the maxillary and the nasal process, the borders of the nasolacrimal groove, and the mandibular process. In the nasal prominence, the signal is confined to the lateral portion flanking the prospective nostrils. (I) un^{ex}/un^{ex}, skull preparation of an adult male, lateral view. The facial skeleton is reduced in length, in particular the praemaxilla, PM, the maxilla, Mx, and the mandible, Mn. The upper incisors appear steeply inserted and the jaw elements strongly bent toward each other, preventing the incisors to meet. (J, K) Thymus phenotypes of newborn wildtype and *undulated* mice. Hematoxylin/eosin-stained 8-μm frontal sections, representing the widest extension of the thymus. Anterior is to the left. The scale bar in (J) represents 200 μm in (J, K); Me, medulla; Cor, cortex. (J) +/+. (K) un^{ex}/un^{ex}. The size of the thymus is drastically reduced. The arrows indicate cysts.

6

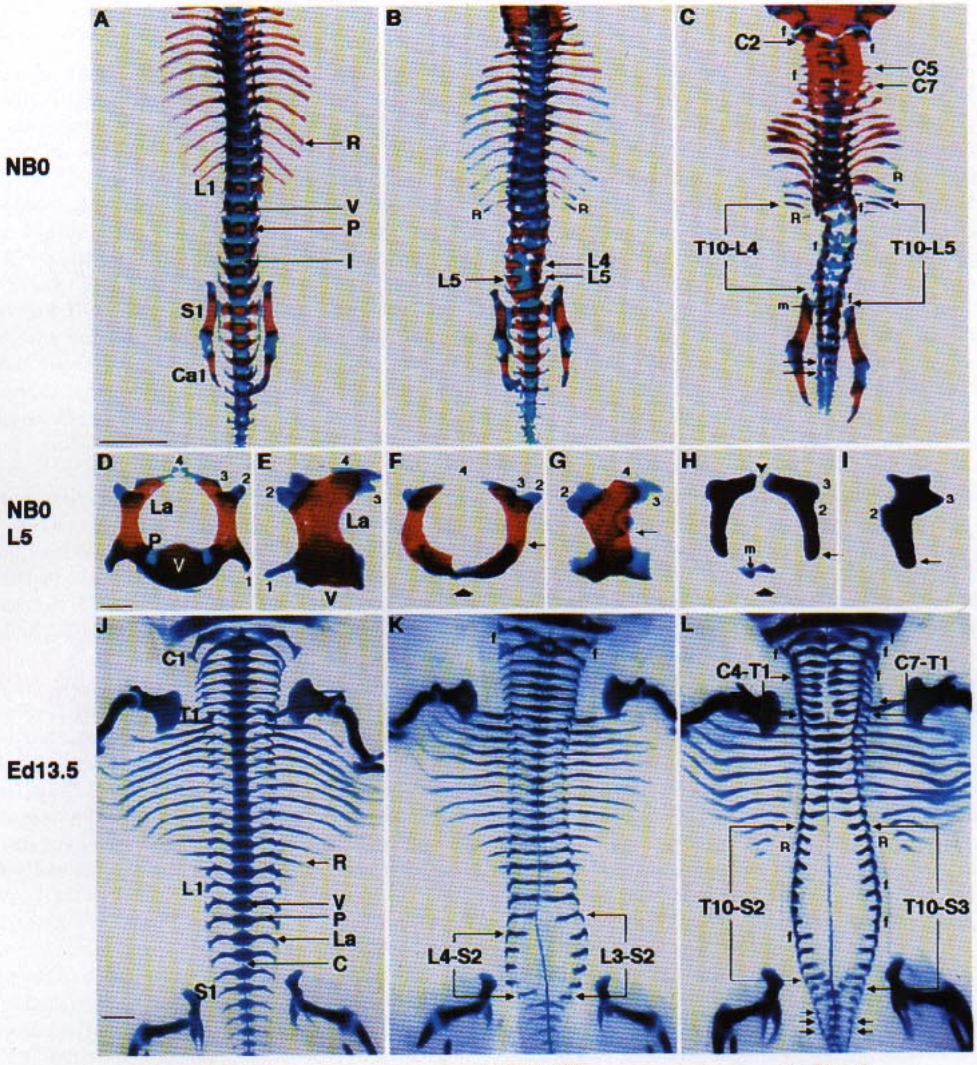
NB0
NB0
L5
Ed13.5
A
B
C
R
L1
V
P
I
S1
Ca1
L5
L4
L5
C2
C5
C7
T10-L4
T10-L5
D
E
F
G
H
I
La
P
V
J
K
L
C1
T1
L1
La
C
S1
L4-S2
L3-S2
C4-T1
C7-T1
T10-S2
T10-S3
+/+
un^ex/un^ex
Un^s/Un^s

7

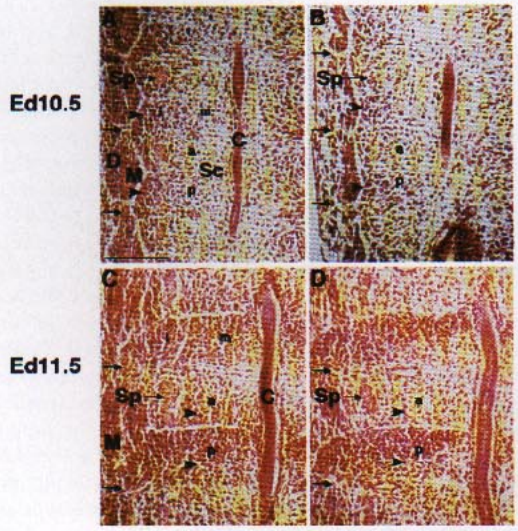
Ed10.5
Ed11.5
A
B
C
D
Sp
M
Sc
+/+
un^ex/un^ex
un/un

8

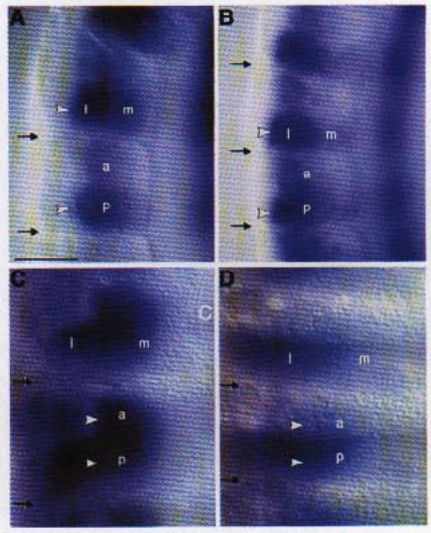
A
B
C
D
l
m
a
p
+/+
un^ex/un^ex
un/un

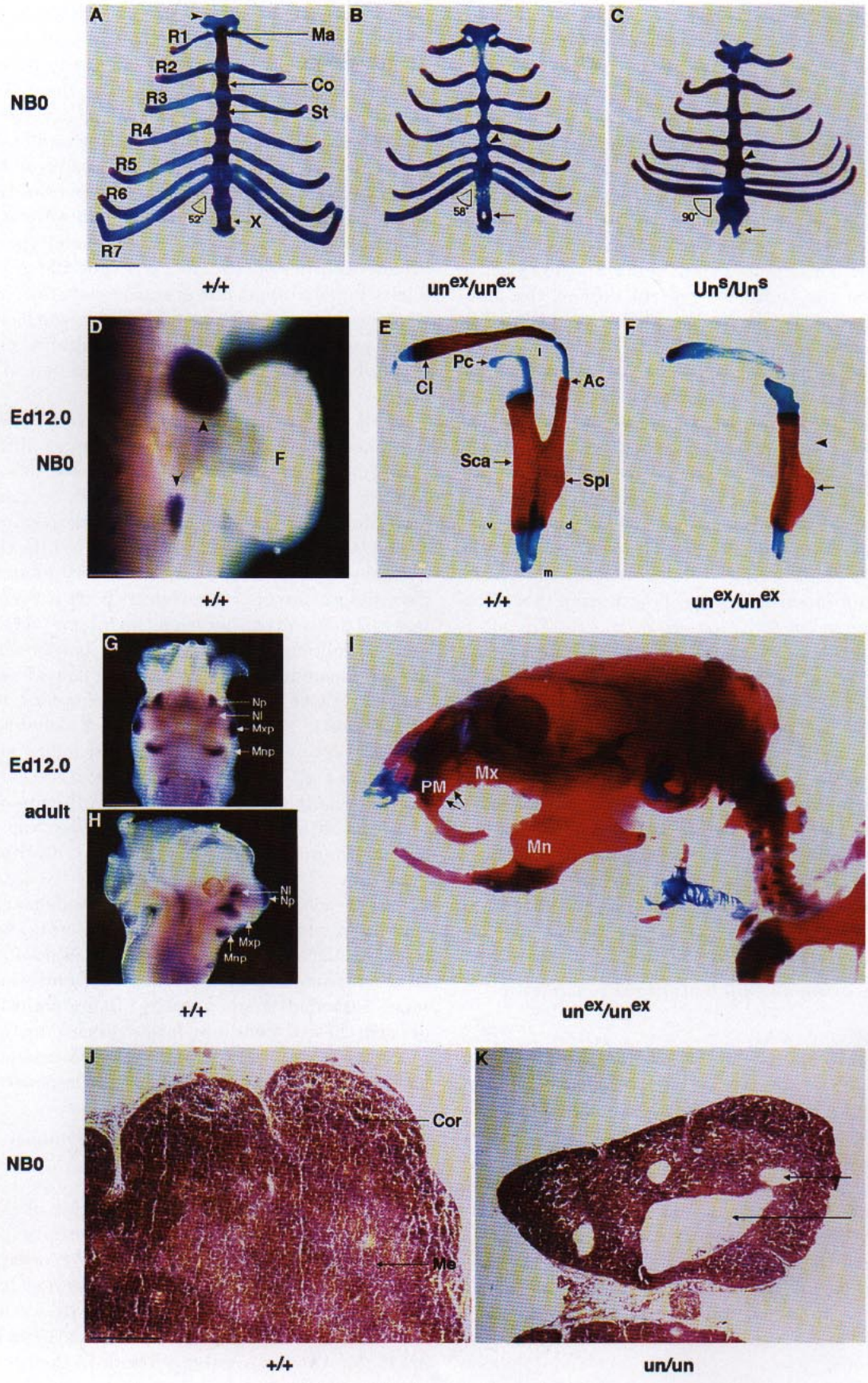
A
R1
R2
R3
R4
R5
R6
R7
Ma
Co
St
X
52°
B
58°
C
90°
NB0
+/+
un^ex/un^ex
Un^s/Un^s
D
A
F
E
Pc
Cl
Ac
Sca
Spl
v
d
m
F
Ed12.0
NB0
+/+
+/+
un^ex/un^ex
G
Np
Nl
Mxp
Mnp
H
Nl
Np
Mxp
Mnp
I
Mx
PM
Mn
Ed12.0
adult
+/+
un^ex/un^ex
J
Cor
Me
K
NB0
+/+
un/un

iniscent of some properties of $Un^s/+$ animals. More obvious than in the previous constellations, the vertebral reductions reach the dorsal aspect of the vertebral column: the processes forming the articulation are poorly structured and often fused to their neighbors, while dorsally shortened neural arches and absent spinous processes result in dorsal vertebral dyssymphyses (Figs. 6H and 6I). This phenotype is a constant feature of Un^s/Un^s animals, which with respect to quantitative differences represent the most extreme case: caudal vertebrae entirely lack the dorsalmost components. In the thoracolumbar region the complete ventral half of the axial skeleton is absent, removing the pedicles, and in addition the 13th pair of ribs.

In posterior body regions of un/Un^s, un^{ex}/Un^s and Un^s/Un^s newborns, more obvious than in $Un^s/+$, the loss of ventrolateral vertebral components occurs independent from the ventromedial: the lower sacral and the caudal regions frequently lack the pedicles while the vertebral bodies reappear, thereby generating retrosomatic clefts that in combination with the dorsal dyssymphyses apply a trifurcated structure to the tail (Fig. 6C). Here, the neighboring vertebral rudiments are totally fused, diminishing the tail length even more dramatically than in $Un^s/+$.

Skeletal preparations of un/Un^s, un^{ex}/Un^s, and Un^s/Un^s embryos confirmed that in all *undulated* mutants the regions of sagittally split vertebrae are most extended at Day 12.5 pc (Fig. 6L, Table 1). Nevertheless, the number of split vertebrae does not differ as drastically from Day 13.5 pc and the newborn stage as in the previous constellations, indicating that pedicle elongation does not as efficiently balance the loss of the ventromedial vertebral column components. As in newborns, Un^s/Un^s embryos are most strongly affected, presenting tail shortening and kinks already at Day 13.5 pc (not shown).

Analysis of Sclerotome Differentiation in undulated Mutants

The vertebral column analysis of *undulated* mutant mice demonstrates that all alleles develop semidominant phenotypes, reducing or extinguishing mainly ventromedial vertebral components. Nevertheless, also lateral and dorsal components are reduced, although to less extent. Grouping the mutants according to qualitative and quantitative criteria, *un* and un^{ex} seem to develop similar phenotypes that differ from all combinations of the Un^s- allele. In order to identify when and by which process the mutant phenotypes are generated, we investigated the lumbar embryonic axial skeletons at the mesenchymal stage on coronal, hematoxylin/eosin stained sections.

In wildtype control embryos at Day 10.5 pc the differentiation of the lateral portion of the sclerotome begins, leading to a less cell dense anterior somite half which will promote neural outgrowth, and the cell dense anlage of the neural arch (Fig. 7A; for review see Christ and Wilting, 1992). In un/un, un^{ex}/un^{ex}, and Un^s/Un^s embryos at Day 10.5 pc, cells in the posterior half of the lateral sclerotome are less densely packed than in the wildtype (Fig. 7B). Moreover, both sclerotome halves appear improperly separated. Both phenotypes are most pronounced in Un^s/Un^s animals (not shown). The similarity in phenotype, however, suggests that in all *undulated* mutants the cell accumulation in the posterior half of the segment is compromised by a similar mechanism, probably accounting for the observed neural arch phenotypes.

At Day 11.5 pc, in wildtype embryos the ventromedial (perichordal) portion of the sclerotome differentiates (Fig. 7C): the lateral band of condensed tissue expands towards the midline. Anteriorly, a new condensation independently arises, encompassing the posterior aspect of the anterior sclerotomal sector. While the densely packed cells will later on give rise to the intervertebral disc, the anlage of the vertebral body is formed by the less cell dense areas between the intervertebral disc anlagen, probably incorporating the borders of the condensed tissue including the ventral neural arch elongation (Dalgleish, 1985; Bagnall and Sanders, 1989; Ewan and Everett, 1992; Goldstein and Kalcheim, 1992). In Day 11.5 pc un/un, un^{ex}/un^{ex}, and again slightly enhanced in Un^s/Un^s animals the lateral cell condensation is still incompletely separated from the anterior region of the somitic segment, however appearing now more defined than at Day 10.5 pc (Fig. 7D). As this zone progresses ventromedially, it narrows to a small band hardly reaching the notochord. Condensation of the sclerotome anterior to the intrasegmental border does not take place yet, indicating that in *undulated* mutants the ventromedial sclerotome differentiation is even more retarded than laterally. Being improperly condensed, these tissues may fail to proceed on the pathway of vertebral column formation, as a consequence abolishing ventromedial axial skeleton components.

Relation of Pax-1 Expression and Sclerotome Condensation

To identify whether the condensation of the sclerotomal mesenchyme results from the activity of the *Pax-1* gene, we analyzed the differential *Pax-1* expression in more detail. When the sclerotome emerges from the somite epithelium, *Pax-1* transcripts are evenly distributed within this tissue (Deutsch *et al.*, 1988; Dietrich *et al.*, 1993). About 6 somites anterior to the youngest *Pax-*

1 expressing segment, the molecules accumulate in the posterior half of the lateral sclerotome, preceding the morphologically visible lateral sclerotome condensation (Fig. 8A). About 16 somites further anterior, at Day 11.5 pc confining the lumbosacral region, this signal forms a broadened band, traversing the segment from dorsolateral to ventromedial (Fig. 8C). In addition, the intrasegmentally located condensing zone is strongly stained. Thus, the elevated *Pax-1* signal colocalizes with regions of excessive cell accumulation, encompassing the intervertebral disc and neural arch anlage. In anterior body regions, where the sclerotome differentiation is further advanced, *Pax-1* transcripts medially concentrate on the intervertebral disc anlage and the perichondrium of the vertebral body. Laterally the signal is restricted to the perichondria of the proximal rib and the neural arch, and in addition to the spinal nerve surrounding mesenchyme (not shown). Zones in which cartilage formation began at the expense of proliferation (Wilting, personal communication) do not express the gene anymore.

In the *un/un* and un^{ex}/un^{ex} mutants, the spatial distribution of *Pax-1* transcripts to subportions of the sclerotome in the first place resembles the wildtype pattern. However, at Day 10.5 pc the expression domain in the posterior sclerotome half appears narrowed, reflecting the delay in lateral sclerotome differentiation (Fig. 8B). Similarly, the *Pax-1* expression at Day 11.5–12.0 pc initially shows wildtype properties, but the signal in the posterior sclerotome half regresses to a small stripe, and the intrasegmentally located signal even fades (Fig. 8D). These changes in *Pax-1* expression suggest that the establishment of borders within the sclerotome is independent from *Pax-1*. However, size and shape of the future vertebral column components that result from regionalized cell accumulation seem *Pax-1* dependent.

Analysis of Sternal Phenotypes in undulated Mutant Mice

To test whether mutant phenotypes occur in nonvertebral *Pax-1* expression domains, we studied the sternum, the scapula, the skull, and the thymus of *undulated* mutant mice. The sternum, except the sternum–rib junctions, has been shown to express *Pax-1* at Day 14.5 pc of development (Deutsch *et al.*, 1988). In addition, occasional fusions of sternebrae have been found in *un/un* (Grüneberg, 1963), suggesting a role of the *Pax-1* gene for the development of this structure. Therefore, the skeletal preparations of the newborn mutant mice were analyzed for rib-cage phenotypes as well (Table 2).

In *un/+* and $un^{ex}/+$ animals, sternebrae may be expanded at the expense of the cartilage zone usually found at the sternum–rib joint. However, the frequency of this phenotype resembles C57bl/6 mice. Nevertheless, compared to wildtype mice, the angle between sternum/xiphoid process and the 7th rib widens from 50 to 52 to 53 to 57 degrees. In *un/un*, un^{ex}/un^{ex}, and un/un^{ex} animals the expansion of sternebrae is more profound (Fig. 9B); 17% of these segments fuse with their neighbors. The angle between xiphoid process and 7th rib increases to on average 58 degrees. In about 54% of these mutants, the ultimate end of the xiphoid process is medially split, probably due to incompletely fused sternal bands. This phenotype is more pronounced in $Un^s/+$, un/Un^s, and un^{ex}/Un^s mice, where occasionally even anterior portions of the sternal bands remain separated. The 7th rib assesses the anteriorly broadened xiphoid process in an angle between 62 and 70 degrees, while sternebral fusions occur with a frequency of about 25%. Similar phenotypes were observed in Un^s/Un^s homozygotes (Fig. 9C). However, these animals differ from the former by a rectangular arrangement of the xiphoid process and the 3rd–7th ribs.

TABLE 2
STERNAL PHENOTYPES IN *undulated* MUTANTS

Mutant	Stage	Number of animals	% Animals with split xiphoid process/ incompletely fused sternal bands	% Enlarged/fused sternebrae between 2nd and 7th ribs
un/+	NB0	9	33	9
$un^{ex}/+$	NB0	7	29	14
un/un	NB0	3	66	20
un^{ex}/un^{ex}	NB0	7	71	34
un/un^{ex}	NB0	7	25	23
$Un^s/+$	NB0	2	100	40
Un^s/Un^s	NB0	2	100	40
un/Un^s	NB0	5	83	27
un^{ex}/Un^s	NB0	5	100	52

Note. Newborn mice were analyzed for incompletely fused sternal bands or xiphoid processes and the reduction or absence of the cartilage stripe at the sternal junction of the 2nd- to 7th ribs, thus assaying for the enlargement or fusion of sternebrae. It has to be noted that in about 50% of C57bl/6 mice, but in none of the NMRI and $+/+(Un^s)$ controls, the ultimate end of the xiphoid processes was terminally split. In C57bl/6, 6% of the sternebrae also appeared enlarged. Thus, *un/+* and $un^{ex}/+$ mice resembled our sample of wildtype animals.

Analysis of Scapula Phenotypes in undulated Mutants

The sternum analysis supported the idea of a *Pax-1* function besides the vertebral column, as the split xiphoid processes probably reflect a requirement of the gene for the fusion of the contralateral sternal bands (Chen, 1953). In the shoulder girdle, *Pax-1* activity and mutant phenotype are even more clearly connected. Here, *Pax-1* expression begins at Day 10.5 pc at the anterodorsal margin of the forelimb (Dietrich *et al.*, 1993)

TABLE 3
SCAPULA PHENOTYPES IN *undulated* MUTANTS

Mutant	Stage	Number of animals	% Scapulae with acromion: Absent	Reduced >1/2	Reduced <1/2
un/+	NB0	9	0	0	0
	E 13.5	29	0	0	0
	E 12.5	5	0	0	0
un^{ex}/+	NB0	14	0	0	0
	E 13.5	26	0	0	0
	E 12.5	16	0	0	0
un/un	NB0	3	0	0	100
	E 13.5	20	20	40	40
	E 12.5	4	87	13	0
un^{ex}/un^{ex}	NB0	7	86	14	0
	E 13.5	6	42	58	0
	E 12.5	10	100	0	0
un/un^{ex}	NB0	7	0	100	0
	E 13.5	12	8	92	0
	E 12.5	10	60	40	0
Un^{s}/+	NB0	2	0	0	100
	E 13.5	15	0	0	100
	E 12.5	11	0	0	0
Un^{s}/Un^{s}	NB0	2	0	0	100
	E 13.5	5	0	0	100
	E 12.5	3	0	0	100
un/Un^{s}	NB0	5	0	0	100
	E 13.5	8	0	0	100
	E 12.5	7	0	0	100
un^{ex}/Un^{s}	NB0	5	0	0	100
	E 13.5	8	0	0	100
	E 12.5	3	0	0	100

Note. In all animals of Table 1, the acromion was quantitatively analyzed for length (absence, reduction by more, or less than 50% compared to the wildtype length), position with respect to the mediolateral axis of the blade, and presence of a second outgrowth. Note that absence of the acromion is confined to the *un/un*, *un^{ex}/un^{ex}*, and *un/un^{ex}* genotypes. Most frequently, this phenotype is found at embryonic stages. In 100% of the *Un^{s}* mutants, the acromion is located close to the shoulder articulation. Fork-like acromial structures, first visible at Day 13.5 pc, are found in 100% of the *Un^{s}* compound heterozygotes.

which in the chicken is believed to form the acromion and parts of the scapular blade (e.g., Beresford, 1983; Saunders, 1948). One and a half day later a transient expression in the posterodorsal margin appears (Fig. 9D), probably corresponding to the medial component of the scapula (Beresford, 1983; Saunders, 1948). Simultaneously, the same pattern can be observed in the hindlimbs and, in addition, in the carpal and tarsal region of the paws at Day 13.5 and 14.5 pc (not shown). While no anatomical changes could be identified in the pelvic girdle, structures that develop in the region of the anterior forelimb expression domain exhibit mutant phenotypes (Table 3).

In *un/+* and *un^{ex}/+* newborns, compared to the wildtype the spina scapulae appears flattened. This phenotype is preformed at embryonic stages, when at Day 13.5 pc of development the angle formed by the scapula and acromion is reduced (data not shown).

The reduction of the spina scapulae is more pronounced in *un/un*, *un/un^{ex}* and *un^{ex}/un^{ex}* (Fig. 9F). In these mutants, however, the most obvious alteration is a reduction or even complete loss of the acromion, the latter most frequently found in *un^{ex}/un^{ex}*, where the corresponding *Pax-1* expression domain appears narrowed already at Day 12.0 pc (not shown). In all three genotypes, embryos at Days 12.5 and 13.5 pc more frequently lacked the acromion than newborns, suggesting that the phenotype may be compensated similar to the vertebral reductions. Occasionally, the clavicle carried wing-shaped structures at the acromial end that could not be related to the embryonic phenotypes (not shown).

In anterior views on the scapulae of *Un^{s}/+* newborns, the spine appears even, while the length of the acromion is only slightly reduced. In contrast to the former mutants however, the acromion is shifted laterally into that third of the scapula that is closest to the shoulder articulation. In addition, it poorly elevates from the blade of the scapula. This phenotype is preformed already at Day 13.5 pc, when the anlage of the acromion leaves the scapula in a small angle close to the prospective shoulder articulation (data not shown).

Similar to *Un^{s}/+*, the shortened acromion of *un/Un^{s}* and *un^{ex}/Un^{s}* compound heterozygotes arises in a position close to the shoulder. However, instead of remaining a separate structure, it widely fuses with the scapula, most pronounced in *un/Un^{s}* animals. In addition, a second fork-like protrusion is formed, that together with the acromion fuses to the clavicle. This fusion seems to be of secondary origin, since at Day 13.5 pc both acromion and the second spike are separated from the clavicle anlage. At Day 12.5 pc, though the fork-like structure is not visible yet, the acromion is laid down as a conical outgrowth (data not shown).

In newborn *Un^{s}/Un^{s}* animals, the acromion forms a short protrusion close to the shoulder articulation, almost entirely fused to the scapula. At Day 13.5 pc it is represented by a short outgrowth close to the shoulder, twice as wide as in the wildtype, at Day 12.5 pointing medially towards the vertebral column rather than laterally towards the shoulder (data not shown).

Summarizing the scapula analysis, all *undulated* mutants develop anatomical alterations, illustrating the semidominance of the *Pax-1* mutation. As in *un/un*, *un/un^{ex}* and *un^{ex}/un^{ex}* exhibiting the strongest phenotypes the acromion is drastically reduced or absent, *Pax-1* activity seems essential for the outgrowth of this structure.

Analysis of the Facial Skeleton in undulated Mutant Mice

So far we described skeletal alterations that are confined to *Pax-1* expression domains in the trunk of the murine embryo. However, beginning with Day 11.5 pc the *Pax-1* gene is expressed in the lateral portion of the maxillary prominence, followed by the base of the mandibulary component of the first branchial arch and the maxillary edge of the nasolacrimal groove (Dietrich *et al.*, 1993). Adjacent to the latter, a weak staining can also be observed in the nasal prominence. All these expression domains reside in the mesenchyme underlying the surface ectoderm (not shown). The signals enhance and progress anteriorly when at Day 12.0 pc the snout forming components grow out (Fig. 9H). Now, also in the nasal region laterally flanking the prospective nostrils, transcription of the *Pax-1* gene starts (Fig. 9G). At Day 12.5 pc the signal in the upper jaw broadens and ventrally surrounds the eye, where a second, dorsal expression domain appears at Day 13.5 pc (not shown). Here, the eyelid remains positive until Day 14.5 pc (not shown), while in the lower jaw the perichondrium of Meckel's cartilage still expresses the gene (Deutsch, 1990).

The *Pax-1* expression domains in the facial region of the mouse embryo suggest that the gene might play a role for the development of skull elements that for the chicken have been demonstrated to arise from neural crest (Couly *et al.*, 1993). Indeed, in about 5% of adult un^{ex}/un^{ex} homozygotes head phenotypes can already externally be identified by a snubby appearance of the snout and, in addition, by small openings of the eyelids (not shown). The snout morphology is combined either with the absence of one or both upper incisors or with incisor overgrowth. Inspection of alcian blue/alizarin red stained skulls revealed that independent from the teeth phenotype length and shape of the jaws are affected: mandible, maxilla, praemaxilla, and os nasale are reduced in their longitudinal dimension. Particularly the distance between incisors and molar teeth appears reduced, leading to a general shortage of the snout (Fig. 9I). Moreover, upper and lower jaws are bent toward each other, and the angle between praemaxilla and incisors is reduced. In the case where reduction and curvature of the lower jaw exceeds the alteration of the upper, both pairs of incisors fail to meet each other, secondarily leading to indefinite growth.

As adult animals are not available for Un^{s}- homozygotes and compound hetejozygotes, we also investigated the skeletal preparations of the newborn animals to identify whether all *undulated* alleles develop skull phenotypes. In all alleles, the elements of the facial skeleton appear shortened. In addition, the mutants have a tendency to more steeply insert the upper incisors, combined with a pronounced curvature of the jaw elements (Table 4). In extreme cases, most frequent in un^{ex}/un^{ex} homozygotes and all combinations of the Un^{s}- allele, one or both upper incisors were shortened, not protruding from the upper jaw, thus confirming the idea of *Pax-1* affecting the development of the neural crest derived facial skeleton.

TABLE 4
FACIAL SKELETON OF *undulated* MUTANTS

Mutant	Stage	Number of animals	% Animals with steeply inserted, reduced incisors/ bent upper jaw
$un/+$	NB0	9	11
$un^{ex}/+$	NB0	7	0
un/un	NB0	3	33
un^{ex}/un^{ex}	NB0	7	86
un/un^{ex}	NB0	7	57
$Un^{s}/+$	NB0	2	100
Un^{s}/Un^{s}	NB0	2	100
un/Un^{s}	NB0	5	80
un^{ex}/Un^{s}	NB0	5	75

Note. Referring to skull preparations of +/+ newborns as controls, newborn mutants were quantitatively analyzed for steeply inserted and shortened incisors and the curvature of the upper jaw between molars and incisors.

Analysis of Thymus Morphology in undulated Mutants

The analysis of *undulated* phenotypes has shown, that in correlation with *Pax-1* expression domains skeletal elements of both mesodermal and neural crest origin are specifically altered. However, the pharyngeal pouches that stem from endoderm also express *Pax-1* starting at Day 8.25 pc (Dietrich *et al.*, 1993). Since the *Pax-1* signal persists in the pouch 3- to 4-derived thymus until juvenile age (Deutsch *et al.*, 1988), we analyzed size and morphology of this organ in newborn *undulated* and wildtype mice on explanted material and haematoxylin/eosin stained frontal sections. Compared to +/+, the thymus of $un/+$ and $un^{ex}/+$ animals is reduced in size (Table 5). This reduction is more obvious in the corresponding un/un and un^{ex}/un^{ex} homozygotes (Fig. 9K), where the thymus only reaches about two-thirds of the wildtype size. In all mutants, the thymus tissue is interspersed with cell-free regions demarcated by endothelia, probably representing cysts. These cysts may arise by the expansion of lymphatic vessels or by the enhancement of the lobular thymic structure, both a possible consequence of the thymus hypoplasia. In compound heterozygotes the thymus resembles that of un/un and un^{ex}/un^{ex} mice, while reduction and cystic alterations in

TABLE 5
THYMUS PHENOTYPES IN *undulated* MUTANTS

Mutant	Stage	Number of animals	Number of sections	Reduced thymus <8 cysts <240 nm	Reduced thymus >8 cysts >240 nm
un/+	NB0	2	164	+	+
un^{ex}/+	NB0	2	104	+	+
un/*un*	NB0	2	99		+
un^{ex}/un^{ex}	NB0	2	193		+
un/un^{ex}	NB0	2	212	+	+
Un^{s}/+	NB0	1	30	+	
Un^{s}/Un^{s}	NB0	2	212	+	
un/Un^{s}	NB0	2	242		+
un^{ex}/Un^{s}	NB0	2	232	+	+

Note. The thymus of newborn animals was explanted and the size estimated referring to the thymus of +/+ animals as controls. After frontal sectioning and HE staining, the size of the largest sections was measured again. In addition, all sections were analyzed for the maximal number and diameter of cysts.

Un^{s} homo- and heterozygotes appear more similar to *un*/+ and un^{ex}/+ (data not shown). Taken together, the *undulated* thymus phenotypes indicate that *Pax-1* influences the development of an organ completely unrelated to skeletal structures.

DISCUSSION

Almost one century of mouse genetics has led to an impressive collection of developmental mutants that may serve as model organisms for the embryonic development of vertebrates (Lyon and Searle, 1989). Unfortunately, the genetic basis has been identified in comparatively few mutants, leaving the genetic control of vertebrate embryogenesis compared to *Drosophila* still very poorly understood. However, within the murine *Pax* gene family three genes could be linked to classical mouse mutants: in *Small eye* the *Pax-6* gene is mutated, *Splotch* mice carry mutations in the *Pax-3* gene, and in *undulated* mutant mice the *Pax-1* gene is affected (reviewed in Gruss and Walther, 1992).

undulated Mutant Mice: An Allelic Series of Pax-1 Mutants

The genetic basis of *undulated* (*un*) has been demonstrated to be a point mutation in the paired box of *Pax-1*, *in vitro* drastically reducing the DNA binding capacity of the mutant protein (Balling *et al.*, 1988; Chalepakis *et al.*, 1991). Specific alterations of the vertebral column, the sternum, the acromion (Wright, 1947; Grüneberg, 1963), as well as the facial skull and thymus (this study) demonstrate the relevance of the mutation also *in vivo*. However, whether or not this mutation allows some residual *Pax-1* activity, could not be determined due to the unknown *Pax-1* targets.

The identification of *Pax-1* dependent phenotypes profits from the existence of two further alleles, un^{ex} and Un^{s}, which, together with *un*, constitute the allelic series of *undulated* mutants. Un^{s}/Un^{s} mice have been shown to lack the *Pax-1* paired box within their genome, suggesting this deletion mutant to be a null allele (Balling *et al.*, 1992; Wallin *et al.*, 1993). Our Southern analysis proved that the deletion encompasses at least 48.3 kb, eliminating the *Pax-1* gene and 38 kb of flanking sequences. Therefore, the possibility remains that the Un^{s} deletion also removes contiguous genes whose absence might contribute to the phenotype.

The problems in interpreting both the *un* and Un^{s} mutation include difficulties in identifying the solely *Pax-1*-dependent *undulated* phenotypes. Therefore, we characterized genotype and phenotype of the third allele, *undulated extensive*. The structural analysis of the *Pax-1* gene in un^{ex}/un^{ex} homozygotes revealed a deletion of at least 28.2 kb, removing the 5th exon including the poly(A) signal. Consequently, the mutant *Pax-1* transcripts lack the poly(A) tail. As polyadenylation is required for RNA stabilization conferred by the poly(A) binding protein (reviewed in Sachs, 1990), the absence of the poly(A) tract probably accounts for the low *Pax-1* mRNA levels observed in these animals. Since the presence of the poly(A) binding protein promotes translation (Jackson and Standart, 1990; Huarte *et al.*, 1992), the amount of un^{ex}/*Pax-1* protein may be even lower. However, since neither the presence of the mutant protein nor the function of the exon 5 encoded amino acids could be determined, un^{ex} may be considered a null allele as well as a hypomorph. Nevertheless, the similarity of the un^{ex} and *un* phenotypes suggest, that also in un^{ex}/un^{ex} solely the *Pax-1* gene is affected. It furthermore suggests that the reduced amount of *Pax-1* transcripts in un^{ex}/un^{ex} is functionally equivalent to the altered DNA-binding properties of the *un*/*Pax-1* protein. Prob-

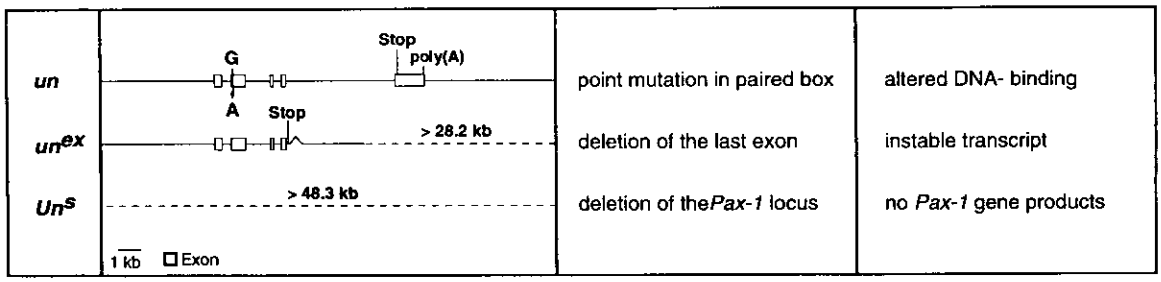

FIG. 10. Mutations in the *Pax-1* gene of *undulated* mutant mice. *undulated* (*un*) mice carry a point mutation in the paired box, altering the DNA binding capacity of the mutant protein. *undulated extensive* (un^{ex}) mice harbor a deletion of at least 28.2 kb, removing the terminal exon and the poly(A) signal. Consequently, the un^{ex}/*Pax-1* transcripts lack the stabilizing poly(A) tail, leading to a drastically reduced amount of transcripts probably due to accelerated turnover. In *Undulated short tail* (Un^{s}) a deletion of at least 48.3 kb encompasses the entire *Pax-1* locus and about 38 kb of flanking sequences.

ably, both mutations similarly reduce the amount of *Pax-1* protein effectively interacting with its targets.

In undulated Mutant Mice Vertebral Components Are Reduced or Absent

The molecular analysis has shown that in all *undulated* alleles the *Pax-1* gene is mutated (Fig. 10). Consequently, phenotypic features shared between these three alleles should reflect the fundamental functional *Pax-1* requirement during the development of the affected structures. The most obvious alteration of *undulated* compared to wildtype mice is the vertebral column phenotype, externally visible as a shortened, kinky tail (Wright, 1947; Balling *et al.*, 1992). A closer examination of the mutant axial skeletons in newborn animals and embryos at Days 12.5 and 13.5 pc revealed that the shortening of the tail results from vertebral malformations rather than the truncation of the axial skeleton: in homozygous *undulated* mutants as well as in the compound heterozygotes, the vertebral bodies are reduced or absent along the entire anteroposterior axis. In addition, the animals may lack the transverse processes at least in the lumbosacral region while the neural arches appear narrowed. Here, in Un^{s} homo- and compound heterozygotes, the pedicles may be absent while the articulation processes appear irregular and the lamina of the neural arches shortened. Thus, in *undulated* mutants all vertebral elements may be compromised. As even *un*/+ and un^{ex}/+ animals may develop mutant phenotypes, the three types of *undulated* mutations have to be qualified as semidominant and *Pax-1* as haploid insufficient.

In all combinations of the Un^{s} allele, one focus of vertebral malformations is confined to the tail, where in Un^{s} homo- and compound heterozygotes the vertebrae may be deprived from the pedicles independent from the vertebral bodies. However, in all *undulated* alleles, at least in the trunk, the extent of vertebral reductions progresses in a gradient-like fashion: with respect to the anteroposterior body axis, the severity of vertebral malformations increases toward the lumbosacral region. Here, the largest somites and subsequently the most massive vertebrae are formed, probably requiring the highest amount of *Pax-1* gene products. Within individual vertebrae, the extent of vertebral malformations progressively enhances from dorsal to ventral, suggesting that the reductions differ only by quantitative means. Thus, *Pax-1* may affect ventral and dorsal vertebral column components by a similar mechanism.

The undulated Vertebral Column Phenotypes Can Be Traced Back to a Delay in Sclerotome Condensation

The idea of a uniform *Pax-1* function for the development of the various vertebral structures is supported by the early *undulated* phenotypes at the mesenchymal stage of vertebral column formation. In wildtype animals, the first sign of sclerotome differentiation is visible at Day 10.5 pc when in the posterolateral portion of the somitic segments the sclerotome cells accumulate in order to form the anlage of the neural arch (for review see Christ and Wilting, 1992). In *undulated* mutants, even earlier than previously reported (Grüneberg, 1954), this zone appears narrowed, less cell dense and less clearly separated. However, the cell density enhances until Day 11.5 pc. At that stage, in wildtype embryos also the morphologically defined ventromedial sclerotome differentiation begins. Here, cells within the posterior segment half proliferate at higher rates (J. Wilting, personal communication), forming a stripe of condensed tissue laterally continuous with the neural arch anlage. Independently, the mesenchyme anterior to the cell dense band condenses and medially unites with the former. In *undulated* mice, both condensations are again affected: the posterior one narrows to a small stripe hardly reaching the notochord, while the intrasegmentally located condensation is not visible at all. Since

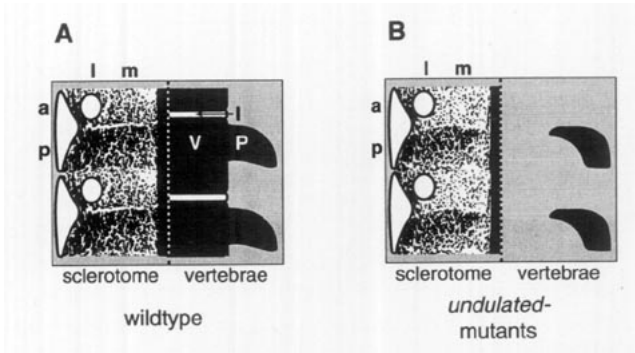

FIG. 11. Model for the formation of the vertebral body, shown by a schematic representation ventromedial embryonic sclerotomes at Day 11.5 pc (left side) and the corresponding vertebral elements (right). The positions of the spinal nerves and the dermomyotomes are indicated by triangularly and oval-shaped white areas, respectively. The black, vertical bar symbolizes the notochord. The cell density within the sclerotomal mesenchyme is represented by the density of dots; l, lateral; m, medial, a, anterior; p, posterior; V, vertebral body; P, pedicle; I, intervertebral disc. (A) In wildtype animals, the cell-dense area in the posterior sclerotome half unites with the noncondensed anterior zone of the adjacent segment and most likely the borders of the intrasegmentally situated condensation in order to form the vertebral body. (B) In *undulated* animals, particularly the medial sclerotome condensations appear delayed. In the lumbar region, the critical cell density may not be reached preventing vertebral body development.

some cell accumulation appears at later stages, both medial and lateral sclerotome condensation can be regarded as delayed rather than abolished. This delay together with the expression of *Pax-1* in the embryonic sclerotome qualifies the condensations as an intrinsic, *Pax-1* dependent program of the sclerotome.

The Sclerotomal undulated Phenotype Suggests a Model for the Development of the Vertebral Body

The interpretation of *Pax-1* mutations to retard sclerotome condensation provides us with a possible scenario for the formation of the vertebral body (Fig. 11): in wildtype mice, this structure is believed to arise from the noncondensed area within the anterior portion of the medial sclerotome (reviewed in Christ and Wilting, 1992). Absolute and relative expansion of this less cell dense zone (Dalgleish, 1985; Bagnall and Sanders, 1989; Gasser, 1979), as well as the contribution of two somites to one vertebral body (Bagnall *et al.*, 1989; Ewan and Everett, 1992; Goldstein and Kalcheim, 1992), suggest that the vertebral bodies incorporate also parts of the medial condensed tissue. This hypothesis is supported by the *undulated* phenotypes: the massive delay in the medial sclerotome condensation lumbosacrally is incompatible with vertebral body formation.

The medial sclerotome condensation itself, however, is composed of two, independently proliferating zones. The first one is located in the posterior half of the somitic segment, continuous with the lateral neural arch anlage. This continuity is particularly obvious at Day 12.5 pc, when the cartilage precursor of the neural arch accesses the notochord, not yet uniting with the adjacent, medial cartilage elements. Therefore, it seems likely that the posterior medial condensation contributes to the anterior portion of a vertebral body. The second medial condensation resides intrasegmentally, contiguous with the former. It posteriorly overlaps with the cartilage element that anteriorly aligns the neural arch elongation, thus possibly contributing to the same vertebral body. In anterior direction, the intrasegmental condensation overlaps with the cartilage element in the anterior segment half, and may therefore also contribute to the adjacent vertebral body. In summary, in agreement with the data obtained from transplantation experiments in the chick (Goldstein and Kalcheim, 1992) we suggest that the vertebral body consists of two, more likely three medial sclerotomal components, the condensed posterior sclerotome half, the noncondensed anterior portion of the adjacent somite, and possibly parts of the flanking, intrasegmentally located condensations, the last also supplying the intervertebral disc anlagen.

In undulated Mutants, Additional Morphological Changes Correspond to Pax-1 Expression Domains

Apart from the vertebral column, additional phenotypic alterations in *undulated* mutant mice could be attributed to *Pax-1* expression domains. The developing sternum represents a *Pax-1* expression domain that originates from lateral mesoderm (Chen, 1952). Here, *undulated* mutants show sternebral fusions, an increased angle between the lowest ribs and the xiphoid process, and a terminally split sternum. The impaired sternal segmentation and the altered sternum-rib assessment may be consecutive to the shortened and strongly curved ribs, thus resulting from the sclerotome deficiency (Chen, 1953). However, the broadened and split xiphoid process may be evoked from incompletely fused sternal bands, directly depending on a *Pax-1* function during elongation and unification of the contralateral sternal anlagen (Chen, 1953).

Another mesodermal expression is confined to the developing shoulder region, that for the chicken has been shown to be of somitic origin (e.g., Saunders, 1948; Beresford, 1983). Here, *undulated* mutant mice exhibit reductions of the spina scapulae and the acromion. While *un/un*, un^{ex}/un^{ex}, and un/un^{ex} mutant mice may completely lack the acromion, Un^{s} animals develop this structure, however in close vicinity to the shoulder articulation. In the Un^{s} compound heterozygotes, a second, fork-like protrusion accompanies the acromion, both secondarily fusing with the clavicle. While this pheno-

type illustrates the qualitative differences in the scapular phenotypes of *undulated* mutants, the acromial reduction in *un* and un^{ex} underlines the requirement of *Pax-1* for the development of this appendicular skeletal element.

A *Pax-1* expression domain that has not achieved much attention so far is the developing nasal, maxillary, and mandibular process. However, this region is of particular interest, since the skeletal elements formed here all originate from neural crest (Couly *et al.*, 1993). *undulated* mutant mice show a remarkable size reduction of the facial skeleton, that may prevent the incisors to meet and to become worn down by use. The incisors themselves may be more steeply inserted or absent. In the facial region in addition to skeletal structures the opening of the eyelid may be reduced, corresponding to the *Pax-1* expression in the developing lid from Day 12.5 pc onward.

The thymus constantly expresses the *Pax-1* gene from the pharyngeal pouch stage to juvenile ages (Deutsch *et al.*, 1988; Dietrich *et al.*, 1993), suggesting a role of *Pax-1* even for the development of this endoderm derived organ. This possibility is supported by the *undulated* mutants: in these animals, the thymus is reduced in size. In addition, the tissue is interspersed by cysts, probably a consequence of the thymus hypoplasia.

Do the Morphological Alterations in undulated Mutant Mice Suggest an Integrated Concept of Pax-1 Function during Development?

Based on the skeletal aberrations in the *undulated* mutant, *Pax-1* so far is interpreted to be required fo the correct differentiation of the sclerotome (Grüneberg, 1954; Balling *et al.*, 1988; Balling *et al.*, 1992). However, the comparative analysis of *undulated* phenotypes revealed that besides the vertebral column morphological alterations in the sternum, the scapula, the facial skull and the thymus can be ascribed to *Pax-1* expression domains. The most obvious common feature of the affected structures is a striking reduction in size, while the fundamental organization is maintained. Another possible role of *Pax-1* may therefore be related to growth processes.

In tissue culture experiments, the overexpression of *Pax-1* leads to cell transformation and neoplastic growth (Maulbecker and Gruss, 1993), thus connecting *Pax-1* with cell proliferation. The oncogenic potential of *Pax-1* is abolished, when the *undulated* mutation is introduced into the expression construct (Maulbecker and Gruss, 1993). In the embryonic sclerotome, *Pax-1* is predominantly expressed in the condensing areas, zones of high mitotic activity (J. Wilting, personal communication). In *undulated* mutants, these zones prematurely narrow, reflecting the delayed cell accumulation. These findings together with the tissue culture data suggest that *Pax-1* mutations may similarly reduce proliferation *in vitro* and *in vivo*. As proliferation is not completely inhibited, the early phenotypes may partly be compensated during development as observed particularly for the heterozygotes. In case the condensations do not reach a critical threshold, the corresponding structures may fail to chondrify. Such a mechanism has already been proposed, e.g., by Grüneberg (1963), and may account for the agenesis of lumbar vertebral bodies and intervertebral discs and the absence of the acromion in *undulated* mutant mice.

We are indebted to Rudi Balling whose work on the *undulated* mutants laid the basis for this study. We gratefully thank Jörg Wilting for sharing information prior to publication. We also thank Michael Kessel, Frank Schubert, Patrick Tremblay, and Rüdiger Fritsch for critically reading the manuscript and for many inspiring discussions, and particularly Frank Schubert for his help on the computer work and the statistical analysis of the *undulated* mutant phenotypes. We are grateful to Alfred Schauer for commenting on the *undulated* thymus phenotypes, to Kirsten Backs for her assistance on the histological analyses, and to Heidemarie Wegener, Peter Goldmann, and Ralf Altschäffel for the photographic work. S.D. was supported by the Deutsche Forschungsgemeinschaft and Max-Planck-Society.

Note added in proof. Recently, two related studies have been published by J. Wallin *et al.* (1994), *Development* **120**(5), 1109–1121, and P. M. Timmons *et al.* (1994), *Development* **120**(10), 2773–2785, describing the *undulated* vertebral column and scapula phenotypes, respectively.

REFERENCES

Ausubel, F. M., Brent, R., Kingston, R. E., Moore, D. D., Seidman, J. G., Smith, J. A., and Struhl, K. (1987). "Current Protocols in Molecular Biology." Wiley, New York.

Bagnall, K., Higgins, S., and Sanders, E. J. (1989). The contribution made by cells from a single somite to tissues within a body segment and assessment of their integration with similar cells from adjacent segments. *Development* **107**, 931–943.

Bagnall, K. M., and Sanders, E. J. (1989). The binding pattern of peanut lectin associated with sclerotome migration and the formation of the vertebral axis in the chick embryo. *Anat. Embryol.* **180**, 505–513.

Balling, R., Deutsch, U., and Gruss, P. (1988). *Undulated*, a mutation affecting the development of the mouse skeleton, has a point mutation in the paired box of *Pax-1*. *Cell* **55**, 531–535.

Balling, R., Lau, C. F., Dietrich, S., Wallin, J., and Gruss, P. (1992). *Development of the skeletal system. In* "Postimplantation Development in the Mouse," pp. 132–143. Wiley, Chichester.

Beresford, B. (1983). Brachial muscles in the chick embryo: The fate of individual cells. *J. Embryol. Exp. Morphol.* **77**, 99–116.

Blandova, Y. R., and Egorov, I. U. (1975). Sut allelic with *un*. *Mouse News Lett.* **52**, 43.

Carrazana, E. J., Pasieka, K. B., and Majzoub (1988). The vasopressin mRNA poly(A) tract is unusually long and increases during stimulation of vasopressin gene expression in vivo. *Mol. Cell. Biol.* **8**, 2267–2274.

Chalepakis, G., Fritsch, R., Fickenscher, H., Deutsch, U., Goulding, M., and Gruss, P. (1991). The molecular basis of the *undulated/Pax-1* mutation. *Cell* **66**, 873–884.

Chen, J. M. (1952). Studies on the morphogenesis of the mouse sternum. II. Experiments on the origin of the sternum and its capacity of self-differentiation *in vitro*. *J. Anat.* **86**, 387–401.

Chen, J. M. (1953). Studies on the morphogenesis of the mouse sternum. III. Experiments on the closure and segmentation of the sternal bands. *J. Anat.* **87**, 130–149.

Chomczynski, P., and Sacchi, N. (1987). Single-step method of RNA isolation by acid guanidinium thiocyanate-phenol-chloroform extraction. *Anal. Biochem.* **162**, 156–159.

Christ, B., and Wilting, J. (1992). From somites to vertebral column. *Ann. Anat.* **174**, 23–32.

Church, G. M., and Gilbert, W. (1984). Genomic sequencing. *Proc. Natl. Acad. Sci. USA* **81**, 1991–1995.

Couly, G. F., Coltey, P. M., and Le Douarin, N. M. (1993). The triple origin of the skull in higher vertebrates: A study in quail-chick chimeras. *Development* **117**, 409–429.

Dalgleish, A. E. (1985). A study of the development of thoracic vertebrae in the mouse assisted by autoradiography. *Acta Anat.* **122**, 91–98.

Deutsch, U. (1990). "Identifizierung der Paired-Box-Genfamilie der Maus und Charakterisierung von *Pax-1* als Entwicklungskontrollgen." Ph.D. thesis, Universität Heidelberg.

Deutsch, U., Dressler, G. R., and Gruss, P. (1988). *Pax-1*, a member of a paired box homologous murine gene family, is expressed in segmented structures during development. *Cell* **53**, 617–625.

Dietrich, S., Schubert, F. R., and Gruss, P. (1993). Altered *Pax* gene expression in notochord mutants of the mouse: The notochord is required for the dorsoventral patterning of the somite. *Mech. Dev.* **44**, 189–207.

Ewan, K. B. R., and Everett, A. W. (1992). Evidence for resegmentation in the formation of the vertebral column using the novel approach of retroviral-mediated gene transfer. *Exp. Cell Res.* **198**, 315–320.

Featherstone, J. M., and Turner, P. C. (1991). Isolation of a gene from *Xenopus borealis* containing a paired box. *Biochem. Soc. Trans.* **20**, 29S.

Feinberg, A. P., and Vogelstein, B. (1983). A technique for radiolabeling DNA restriction endonuclease fragments to high specific activity. *Anal. Biochem.* **132**, 6–13.

Gasser, R. F. (1979). Evidence that sclerotomal cells do not migrate medially during embryonic development of the rat. *Am. J. Anat.* **154**, 509–524.

Goldstein, R. S., and Kalcheim, C. (1992). Determination of epithelial half-somites in skeletal morphogenesis. *Development* **116**, 441–445.

Grüneberg, H. (1954). Genetical studies on the skeleton of the mouse. XII. The development of *undulated*. *J. Genet.* **52**, 441–455.

Grüneberg, H. (1963). "The Pathology of Development." Blackwell, Oxford.

Gruss, P., and Walther, C. (1992). *Pax* in development. *Cell* **69**, 719–722.

Huarte, J., Stutz, A., O'Connell, M. L., Gubler, P., Belin, D., Darrow, A. L., Strickland, S., and Vassalli, J.-D. (1992). Transient translational silencing by reversible mRNA deadenylation. *Cell* **69**, 1021–1030.

Jackson, R. J., and Standart, N. (1990). Do the poly(A) tail and 3′ untranslated region control mRNA translation? *Cell* **62**, 15–24.

Kaufman, M. (1992). "The Atlas of Mouse Development." Academic Press, New York.

Kessel, M., Balling, R., and Gruss, P. (1990). Variations of cervical vertebrae after expression of a *Hox-1.1* transgene in mice. *Cell* **61**, 301–308.

Lyon, M. F., and Searle, A. G. (1989). "Genetic Variants and Strains of the Laboratory Mouse," pp. 1–876. Oxford Univ. Press, Oxford.

Maulbecker, C. C., and Gruss, P. (1993). The oncogenic potential of *Pax* genes. *EMBO J.* **12**, 2361–2367.

Plachov, D., Chowdhury, K., Walther, C., Simon, D., Guénet, J.-L., and Gruss, P. (1990). *Pax-8*, a murine paired box gene expressed in the developing excretory system and thyroid gland. *Development* **110**, 643–651.

Romeis, B. (1989). "Mikroskopische Technik." Urban & Schwarzenberg: München/Wien/Baltimore.

Sachs, A. (1990). The role of poly(A) in the translation and stability of mRNA. *Curr. Opin. Cell. Biol.* **2**, 1092–1098.

Saunders, J. W. (1948). The proximo-distal sequence of origin of the parts of the chick wing and the role of the ectoderm. *J. Exp. Zool.* **108**, 363–404.

Stamminger, T., Fickenscher, H., and Fleckenstein, B. (1990). Cell type-specific induction of the major immediate early enhancer of human cytomegalovirus by cyclic AMP. *J. Gen. Virol.* **71**, 105–113.

Wallace, M. E. (1979). *Mouse News Lett.* **61**, 29.

Wallace, M. E. (1980). *Mouse News Lett.* **63**, 10.

Wallin, J., Mizutani, Y., Imai, K., Miyashita, N., Moriwaki, K., Taniguchi, M., Koseki, H., and Balling, R. (1993). A new *Pax* gene, *Pax-9*, maps to mouse chromosome 12. *Mamm. Genome* **4**, 354–359.

Wilkinson, D. G. (1992). "*In Situ* Hybridisation; A Practical Approach." Oxford Univ. Press, London.

Wright, M. E. (1947). *Undulated*: A new genetic factor in *Mus musculus* affecting the spine and tail. *Heredity* **1**, 137–141.